# LAMONT-DOHERTY GEOLOGICAL OBSERVATORY

## OF COLUMBIA UNIVERSITY

*PALISADES, NEW YORK*



Doc 1473

## Long-Period Seismological Research Program

**Final Report**

**Contract F44620-71-C-0082**

**Approved for public release; distribution unlimited**

**30 June 1976**

**Sponsored by**

**Advanced Research Projects Agency**

**ARPA Order No. 1827**

| | |
|---|---|
| ARPA Order Number: | 1827 |
| Program Code Number: | 3F10 |
| Contractor: | Columbia University |
| Effective date of contract: | 15 March 1971 |
| Contract expiration date: | 30 April 1976 |
| Amount of contract: | $958,231.00 |
| Contract number: | F44620-71-C-0082 |
| Principal Investigator: | Lynn R. Sykes, 914-359-2900 x 280 |
| Program Manager: | Donald W. Forsyth, 914-359-2900 x 387 |
| Project Scientist: | William J. Best, 202-693-0162 |
| Title of Work: | Long-Period Seismological Research Program |

# DISCLAIMER NOTICE

THIS DOCUMENT IS THE BEST QUALITY AVAILABLE.

COPY FURNISHED CONTAINED A SIGNIFICANT NUMBER OF PAGES WHICH DO NOT REPRODUCE LEGIBLY.

TABLE OF CONTENTS



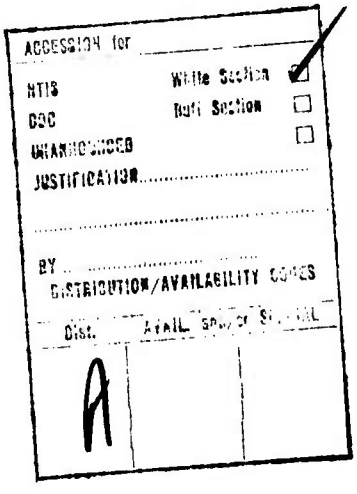

## SUMMARY

During the first year of the subject contract, five high-gain, long-period (HGLP) seismograph stations were maintained and a sixth station was installed and maintained. During the second year, responsibility for maintenance was transferred to the Albuquerque Seismological Center. In succeeding years, Lamont-Doherty continued operating the high-gain station at Ogdensburg, New Jersey (OGD). Research completed under this contract included investigation into the characteristics of long-period earth noise, the detection capabilities of the high-gain stations, digital signal enhancement techniques, and new methods of distinguishing earthquakes from underground explosions, as well as several studies in general seismology using high-gain data.

A detailed study of earth noise at all 11 HGLP sites found that the spectra of earth noise at each site is characterized by a minimum in the period range 25 to 45 seconds. The level of earth noise recorded by vertical seismographs is independent of local meteorological conditions, but at shallow sites, the earth noise levels recorded by horizontal seismographs exhibit a diurnal cycle associated with daily variations of atmospheric turbulence. The horizontal earth noise associated with atmospheric turbulence is attenuated by overburden to about 10% of the surface noise level at a depth of about 150 m.

An evaluation of the detection capabilities of the HGLP stations showed that surface waves could be observed for 90% of the reported events of $m_b$ 4.2 or larger which occurred within 30° of a station. At distance ranges of 80° to 100°, the detection threshold increases to about $m_b$ 4.7. Roughly half of the 10% not observed are masked by the coda of earlier larger events. The thresholds are expected to be lowered by about 0.2 units if digital processing techniques, such as time-varying adaptive filters, are applied. Polarization and azimuthal filters are capable of a signal-to-noise enhancement of more than 6 db for signals from small events. These filters have proved to be more effective than passive techniques or matched filtering.

A new surface wave magnitude scale based on the amplitude of higher-mode Rayleigh waves was developed and applied to earthquakes and explosions in central Asia. Several anomalous events in central Asia, which are characterized by unusually low $M_s$:$m_b$ ratios and hence could be suspected to be nuclear explosions, are reclassified as earthquakes when the new, higher-mode scale, $M_s^h$, is employed. The focal depth and mechanism of these anomalous events apparently causes


Next page

poor excitation of the fundamental mode Rayleigh wave without significantly affecting the amplitude of the higher mode. Elimination of these source related factors from traditional $M_S:m_b$ discriminants is an essential tool for reliable discrimination between earthquakes and nuclear underground tests.

In other investigations, surface waves were used to study the focal mechanism of small magnitude events, the pulse distortion of body waves travelling non-minimum time paths was computed, and the use of seismograph arrays in determining earth structure was examined.

# I. STATION MAINTENANCE AND INSTALLATION

## A. MARCH, 1971 TO APRIL, 1972

Maintenance was carried out for the five previously installed high-gain seismograph stations at Charters Towers, Australia (CTA), Fairbanks, Alaska (FBK), Eilat, Israel (EIL), Chiang Mai, Thailand (CHG), and Ogdensburg, New Jersey (OGD), and a sixth high-gain station at Toledo, Spain (TLP) was installed and maintained.

Preparation for the maintenance trips to CTA, FBK, CHG, and EIL began in May 1971. The field teams involved in these trips prepared all the necessary test equipment for foreign shipment and made arrangements for their trips with the different participating institutions. It was necessary to make major modifications to the inverters and battery chargers purchased from the Exide Company as part of the uninterruptable power units to be installed at each site. Inadequate wiring in the battery chargers was corrected and relays and timers were added to the inverters. All necessary additional power cables and electrical equipment (power switches, fuses, relays) were purchased and prepared for shipping.

One man from each team spent as much time as necessary to learn how to perform a complete acceptance test on the Astrodata Digital system. One complete set of spare digital cards and a tape deck were taken to CTA and FBK to repair the digital recorders at those sites. Prior to the maintenance trips, the digital systems at CTA and FBK were inoperative while the header data on the recorder at EIL was incorrect. By the end of the maintenance trips to these three stations, all three digital recorders were working properly.

It had become apparent that most of the failures of the digital recorders incurred since the initial installation of the high-gain stations were a result of the station voltages being either too low or not sufficiently regulated, and repeated failures of the station power (especially at CTA and CHG). Thus, in addition to the uninterruptable power units which were installed at all the sites, new power lines and transformers were installed at CTA and CHG. The uninterruptable power unit, described in more detail in the High-Gain Long-Period Seismograph Station Instrumentation Report (Lamont, 1971), consists of an inverter, battery charger, battery rack, and 20 six volt batteries. Standard tests of the seismograph systems at each site were performed. These tests included redetermination of seismometer and galvanometer free periods, damping characteristics, current sensitivities, and absolute frequency responses of the low and high-gain outputs of the three component systems. Copies of the absolute frequency response determined at that time were forwarded to Texas Instruments and the Seismological Data Center in Asheville, North Carolina, for distribution to users of the high-gain data.

The maintenance teams at CTA and CHG also installed microbarographs and anemometers, obtained at no cost to this contract. Data from these instruments are being used in the study of long-period earth noise at those two sites.

Failure of the Cipher tape decks in the digital recorders at FBK on 22 August 1971 and TLO on 15 September 1971 necessitated special maintenance trips of approximately one week duration to each site. The FBK system was repaired on 30 October 1971 and the TLO system on 5 November 1971. Since these respective times both digital systems have been operational.

The digital recorder at CTA failed for the second time on 29 August 1971. At that time we contacted a digital technician based in Townsville, Australia, to service the CTA system. As of 15 March 1972, after many attempts, he was unable to repair the CTA recorder. Thus arrangements were made to ship a complete new digital unit from Lamont to CTA.

On 26 December 1971, the digital technician from Townsville, Australia, was sent to Chiang Mai, Thailand, to work on the digital recorder at that site, CHG, which had been out of operation since 1 May 1971. He was successful and CHG has been digitally operational since 1 January 1972.

Lamont personnel had, during the time period requested, sent instructions and replacement parts for many tests to be carried out on the digital recorder by personnel responsible for the routine maintenance of the seismic equipment at CHG. All of these attempts were unsuccessful. In fact, it is now evident that station operators at most of the sites, although proficient in their maintenance of the seismograph systems, cannot cope with the complexities of the digital recorders. For this reason we have attempted to contact qualified digital technicians in Spain, Israel, and Thailand who can service the digital recorders in those countries. We feel that this is the most efficient way to maintain these systems.

During the time period 15 July to 17 August 1971, installation of the sixth high-gain station was completed at Toledo, Spain. This station is equipped with a digital recorder and an uninterruptable power unit. The high-gain station is located in a newly excavated tunnel about 4 km from the Toledo Geophysical Observatory. Personnel from the Toledo Observatory, under the direction of Dr. Gonzalo Payo, are responsible for the daily maintenance and record changing of the high-gain station. Peak recording magnifications obtained at this station are: for the vertical 70k at 40 sec; E/W 36k at 47 sec; N/S 36k at 40 sec. The three letter code for this site is TLO.

## B. MAY, 1972 TO APRIL, 1973

The six high-gain seismograph stations previously installed by Lamont were maintained while carrying out an orderly transition of maintenance responsibilities for those stations to the NOAA group at Albuquerque, New Mexico. During May, June, and July of 1972, considerable time was spent preparing for and carrying out combined inspection-maintenance trips to the VLP stations at Charters Towers, Australia (CTA); Chiang Mai, Thailand (CHG); Kipapa, Hawaii (KIP); and Matsushiro, Japan (MAT). As a result of these trips, several recommendations were made for improvements such as: the addition of air-conditioners in the recording rooms at CTA and CHG for more efficient operation of the digital recorders, and instrument repair techniques that should result in greater continuity of the analog data. In addition, personnel at each site were thoroughly advised of the transition of maintenance responsibilities from Lamont to NOAA.

During the last two weeks in April 1972, a two man team from Lamont traveled to Fairbanks, Alaska, to close out the station FBK. All the equipment at that site, including the instrument tanks, were crated and shipped either by truck or airplane to NOAA at Albuquerque. The final recordings from FBK are dated 25 April 1972.

Seismograms and magnetic tapes from all the VLP stations were sent to Lamont up to 1 September 1972 for quality control. As explained in previous reports, the magnetic tape data were examined on a playback system (cathode ray tube) and compared with the seismograms. The NOAA group at Albuquerque was advised of any malfunctions detected. After examining the tapes for quality control the tapes were copied and the originals forwarded to Texas Instruments. The seismograms are sent to VELA Seismological Center before being film chipped in Asheville, North Carolina. Since 1 September the NOAA group at Albuquerque has been copying tapes and sending the original tapes and seismograms directly from Albuquerque to the VELA Seismological Center. There is no back-log of seismograms from any of the stations at Lamont.

## C. MAY, 1973 TO APRIL, 1974

The high-gain station at Ogdensburg, New Jersey (OGD), was maintained in constant operation. The analog (seismograms) data were complete for the entire year. A problem with the zero level of the ADC unit in the digital data acquisition system was corrected by Lamont personnel. This problem resulted in only minimal (two weeks) loss of digital data. A special air conditioned room was constructed on the 1850' level of the mine observatory. This room is 12' long, 5' deep, and 8' high and houses the digital magnetic tape recorder. Controlling the environmental temperature, humidity, and dust content in this manner should ensure continued dependable operation of the digital tape recorder. Seismograms and magnetic tapes from OGD through November 1973 were forwarded to Asheville, North Carolina, for microfilming, and AFTAC in Alexandria, Virginia, respectively. After December 1973 both the seismograms and digital data from OGD were shipped to the Albuquerque Seismological Center in New Mexico.

## D. MAY, 1974 TO APRIL, 1975

The high-gain station at Ogdensburg, New Jersey (OGD) was maintained in constant operation. In late June, the oscillator-discriminator electronics for the north/south seismometer began to function in an erratic manner. A technician was sent from the Albuquerque Seismological Center (ASC) to replace the unit and to recalibrate the entire system with the assistance of Lamont personnel. The digital recorder was also checked and adjusted at this time. This was the first time the instrument pressure tanks had been opened since late in 1971, resulting in a disturbance of the thermal environment. The N/S component remained instrumentally noisy for a period of months but gradually improved.

In late October, occasional spurious transients began to appear on the visual display of the digital records. Personnel from ASC suggested

the ADC unit of the digital recorder might be at fault. Replacement parts were installed, but in early December, the tape deck inexplicably began to shut off intermittently. It finally failed totally and was not restored to operation until two technicians from ASC arrived. At that time, the new solid-state amplifier replacements for the old PTA were also installed. One amplifier failed during installation and was immediately replaced. During the first large earthquake following installation, the magnitude 7.5 event on February 2, 1975 in the Aleutians, the vertical and north/south solid-state amplifiers were apparently oversaturated, and ceased producing useful data. Replacements were sent from ASC, but some high-gain data was unavoidably lost. Prior to failure of the solid-state amplifiers, the records were comparable to the old PTA records.

It is regretable that component failures in the digital system and the high-gain amplifiers led to a considerable loss of data in the last year. Roughly 20% of lost time is attributable to digital tape recorder failure.

Both the seismograms and digital data from OGD have been shipped to ASC in New Mexico.

E. MAY, 1975 TO APRIL, 1976

The high gain station at Ogdensburg, New Jersey has been maintained in constant operation. Approximately 90 photographic seismograms are acquired each week in addition to a magnetic tape once per three weeks. These data are forwarded to the Albuquerque Seismological Center and a copy of the tape is stored in the Lamont Data File. The displacement outputs of the Geotech long-period seismometers are recorded on 2" per hour analogue chart recorders as are the outputs from four quartz-tube strainmeters. We are in the process of transferring the seven chart records to a multichannel 3" per hour recorder.

The routine operation of the observatory has required two full time technicians in the past. From October 1975 we have operated the station with one technician (M. Connor) and have discontinued recording seismic data from levels other than the -560 m level of the mine in which the observatory is located.

The digital recording of the long-period data has been interrupted on a number of occasions by electronic malfunction of the Astrodata recorder. This is now maintained by the Albuquerque Seismological Center who have arranged on site repairs when required.

# II. RESULTS OF DATA ANALYSIS

## A. EARTH NOISE

### 1. Earth Noise Characteristics at High-Gain Stations

Until about 1971 the bulk of the information on earth noise at periods longer than 10 to 20 sec has come from seismograph stations located in the contiguous United States. The 11 high-gain, long-period (HGLP) seismograph stations that were recently installed at several locations around the world are providing important new information on the temporal and spectral behavior of earth noise at periods longer than approximately 10 sec: An important aspect of the HGLP stations is that they are located in a variety of geologic and tectonic settings (Figure 1). In particular, the installation of a HGLP seismograph station at Kipapa, Hawaii (KIP), has enabled us for the first time to examine the characteristics of long-period earth noise at a mid-ocean site.

A major contribution of this study is the significant increase in the number of long-period earth noise spectra that are available from areas other than the contiguous United States. The information presented in this study forms a comprehensive set of data on long-period earth noise which will be useful for various seismological investigations. For example Linde and Sachs (1971) pointed out the importance of taking into account the contribution of noise to the long-period portion of the spectra of seismic waves in any attempt to distinguish between differing theories of earthquake radiation (Archambeau, 1968; Brune, 1970). As a second example, the noise spectra presented in this study pertain to detection and discrimination between earthquakes and underground nuclear explosions in that they provide an estimate of minimum detectable signals, especially surface waves (Rayleigh and Love), as recorded by a single instrument at a particular site. Knowledge of the spatial and temporal characteristics of long-period earth noise would aid in the design (element spacing) of seismic arrays that might further improve the detection capabilities for surface waves.

Digital data samples were selected on the following basis. Initially the analog (photographic paper or 70 mm film chips) seismograms were examined, if they were available, to obtain four to five hours of data during which no reported earthquakes or transient disturbances could be observed. The data sample did not have to be continuous because the program for computing the power spectrum could skip over predetermined time segments. Next the Monthly List of Preliminary Determinations of Epicenters (National Ocean Survey, now U.S. Geological Survey) was checked for occurrence of unobserved earthquakes during the selected time intervals. Finally, the digital data were inspected for transient disturbances by using a cathode ray tube. Thus, it was assured that the data selected for each station were free of earthquakes and spurious transients.

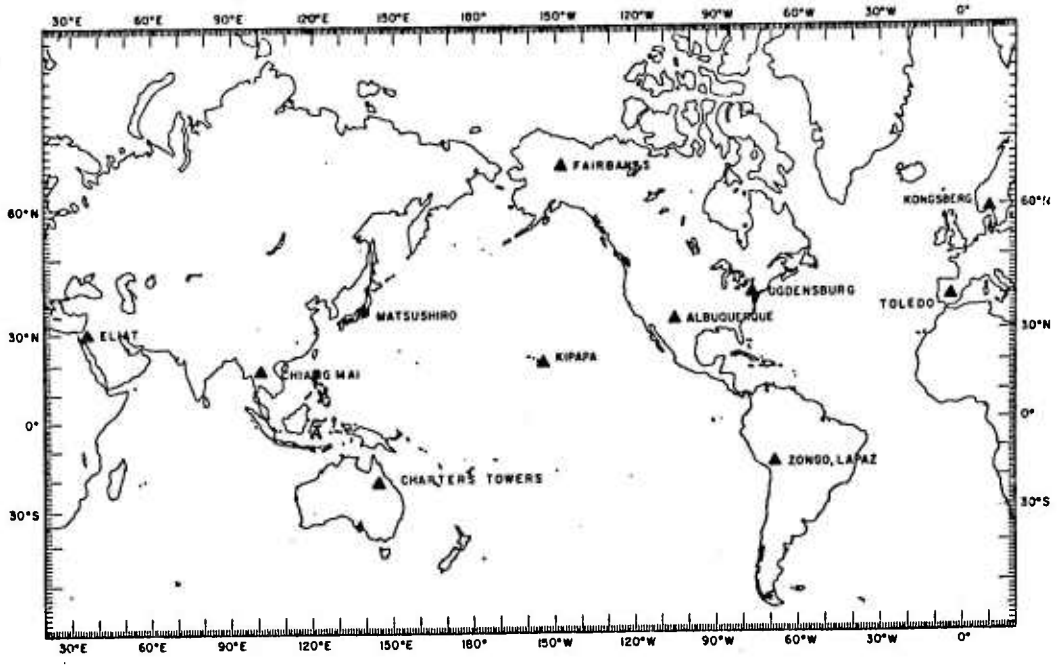


FIG. 1. Map of the world showing the location of the 11 high-gain, long-period stations.

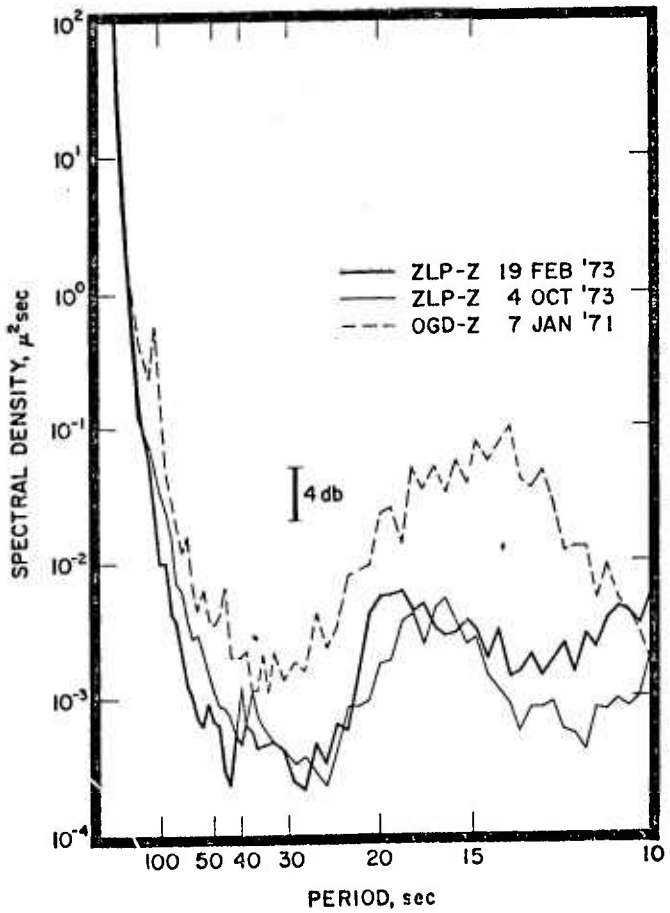


Figure 2.

Earth noise power spectra for the vertical seismographs at OGD and ZLP. The power spectra in all the remaining figures, except figure 11a and b, have been set to their absolute value and corrected for instrumental response. The 90% confidence interval indicated by the error bars is approximately the same for all power spectra presented.

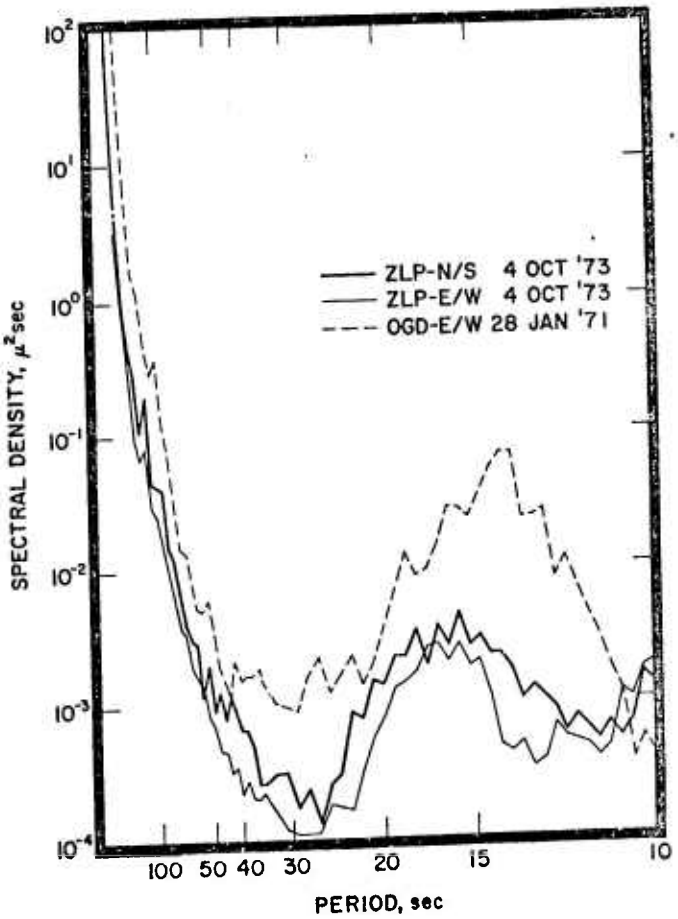


Figure 3.

Earth noise power spectra for the horizontal seismographs at OGD and ZLP.

Each power spectrum was estimated by time-averaging the square of the Fourier coefficients of up to twenty time segments of the data set. Each of the time segments was 1,024 sec long, with the exception of the KON data segments which were 512 sec long. The spectra shown here are corrected for instrument response and set to the absolute level of ground motion unless explicitly noted.

Deep Sites There are four HGLP stations with more than 200 m of overburden above the seismometer vaults. They included OGD, the prototype HGLP station at 543 m, EIL at 200 m, KON at 340 m, and ZLP at 300 m. We will consider OGD and ZLP first; KON will be given special consideration later.

Visual examination of all the available 70 mm film chips from OGD and ZLP shows that the level of vertical earth noise at these two stations is independent of all small-scale meteorological conditions of local origin. In the case of OGD, nearly three years of data were examined. Power spectra typical of background earth noise at OGD and ZLP are shown in Figure 2. These spectra, which are corrected for instrument response, show comparable shapes and absolute levels at periods longer than about 25 sec and show a broad minimum between 25 and 45 sec. At periods shorter than about 20 sec, the OGD spectrum for this particular time interval has higher long-period (16 to 20 sec) microseismic level. The fairly rapid increase (12 to 14 db/octave) in the spectral levels at periods longer than about 50 sec is partially controlled by instrumental noise (Savino et al., 1972; Fix, 1973). By this statement we are referring to the fact that the earth noise spectrum is not a constant level above the instrumental noise of the seismograph system. The 40 sec power of earth noise at OGD is about 20 db above the instrumental power while at about 100 sec the separation is about 10 db. If the instrumental noise of the seismograph system fluctuates with time, it is possible that the instrumental noise may begin to contaminate the earth-noise spectrum at periods longer than about 50 sec.

Analysis of a similar large quantity of data from horizontal seismographs operating at OGD and ZLP indicate that the levels of earth noise recorded by horizontal seismographs are generally independent of local meteorological conditions. In addition as indicated in Figure 3 during ordinary weather conditions, the shape, absolute levels, and the occurrence of a minimum are similar to those shown in power spectra for earth noise recorded by vertical seismographs (Figure 2). There is an indication that the absolute levels of the horizontal power spectra are lower than the absolute level of the vertical spectra during the same time interval.

Shallow Sites There are seven HGLP stations with less than 50 m of overburden above the seismometer vault. First to be considered is CTA (30 m of overburden) since both analog and digital recordings from a single on-site microbarograph are available from this site, permitting a quantitative correlation between local meteorological conditions and earth noise.

Typical examples of power spectra of the earth noise at CTA spanning a two-year time interval are shown in Figures 4a, b, and c. In Figure 4a note the minimum in the spectra between about 30 and 45 sec and that it is stable in absolute level in the passband to within about 6 db for the two-year time interval. The 6 db variation is barely above the 95% confidence limit of 4 db for the power spectra calculations. Also note that for the same time interval that the power in the long-period (16-20 sec) microseism band varied by 12 to 14 db. The minimum in the spectra of horizontal earth noise tends to be broader (25 to 45 sec) and to be less pronounced (Figures 4b and c). In fact, the minimum is nearly filled in by a higher noise level on the horizontal spectra for September 21, 1973. But note that the vertical spectrum is unchanged.

Nearly three years of 70 mm film chips were examined to verify the results given by a limited number of power spectra spread over a two-year time period. The film chip data and the power spectra show that earth noise recorded by the vertical seismograph does not experience any apparent diurnal variations and the 40 sec level of earth noise recorded by the vertical seismograph is unaffected by variations of the 16-18 sec microseism level.

Charters Towers, Earth Noise as Correlated to Microbarograph Noise. Examination of the 70 mm film chips from CTA has made it very obvious that the horizontal earth noise undergoes a very definite diurnal cycle. This cycle characteristically goes from 03:00 → 15:00 noisy to 17:00 → 02:00 quiet (local times). The relative terms "noisy" and "quiet" involve a noise decrease of about 6 db. Figure 5 also shows that the fluctuations in the 40 sec level of the horizontal noise correlate very well with variations in the 40 sec level of the noise recorded by the microbarograph.

Cross-spectra between earth noise recorded by the horizontal seismographs and the atmospheric pressure variations recorded by the single on-site microbarograph were calculated to study the correlation between these two types of noise. The cross-spectra strongly indicate that the variation of local barometric pressure is one of the principal sources of the earth noise recorded by the horizontal seismographs. McDonald et al. (1971) and Priestly (1966) have observed that microbarographs that do not employ properly designed pipe array filters or have no filter at all (the situation of the microbarograph at CTA) are principally sensitive to the atmospheric turbulence in the boundary layer immediately above the earth's surface. Thus, the cross-spectra indicate, more specifically, that atmospheric turbulence in the boundary layer immediately above the earth's surface is a principal source of earth noise recorded by horizontal seismographs.

Significant coherence at periods longer than about 30 sec has been observed during daylight hours between earth noise recorded by the horizontal seismographs and atmospheric pressure variations recorded by the microbarograph (Figure 6b). In addition in Figure 6a note the similar correlation between the earth noise recorded by the two hori-

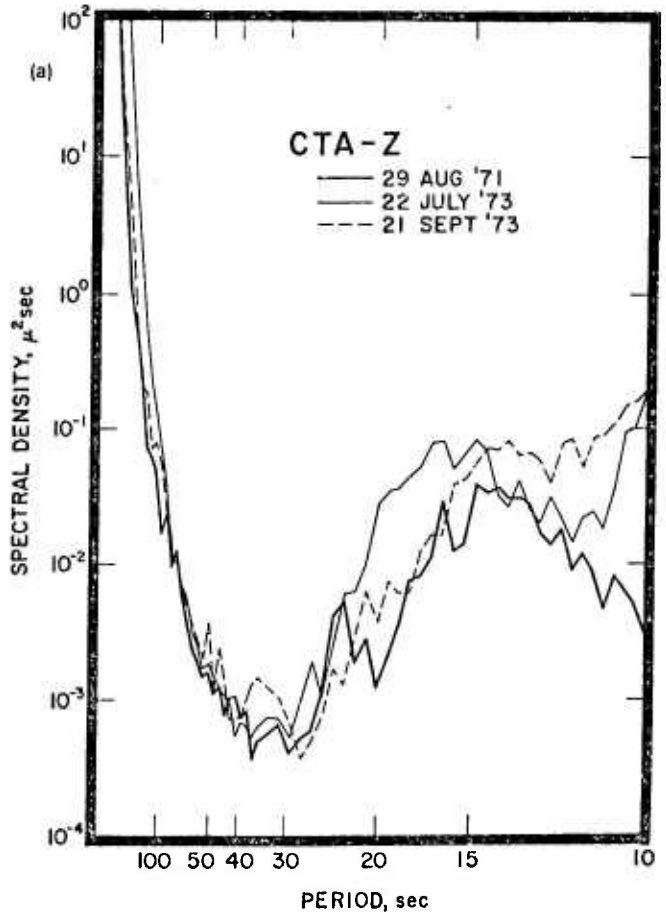


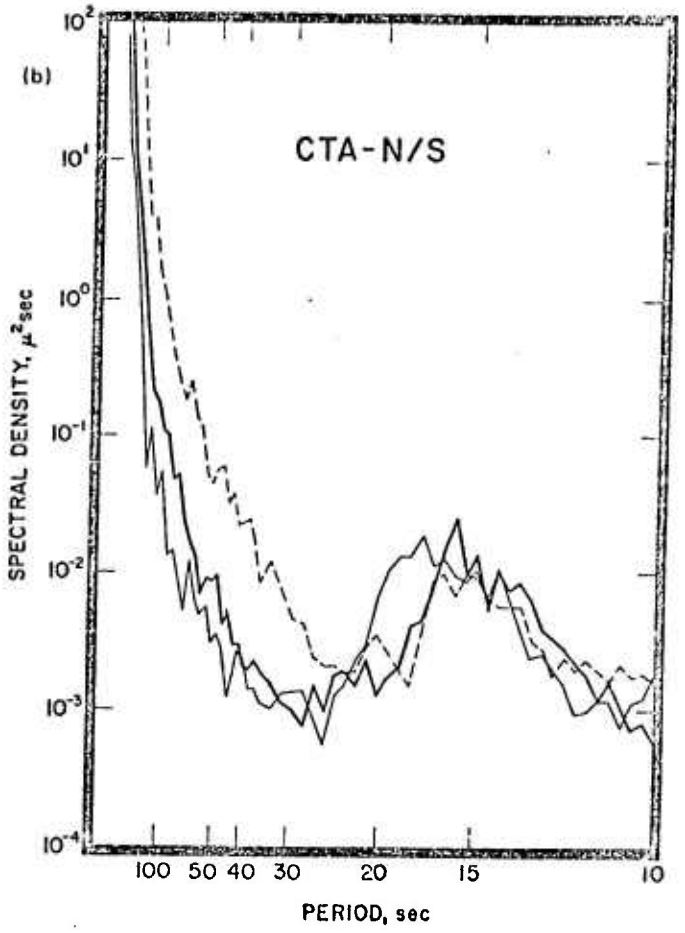


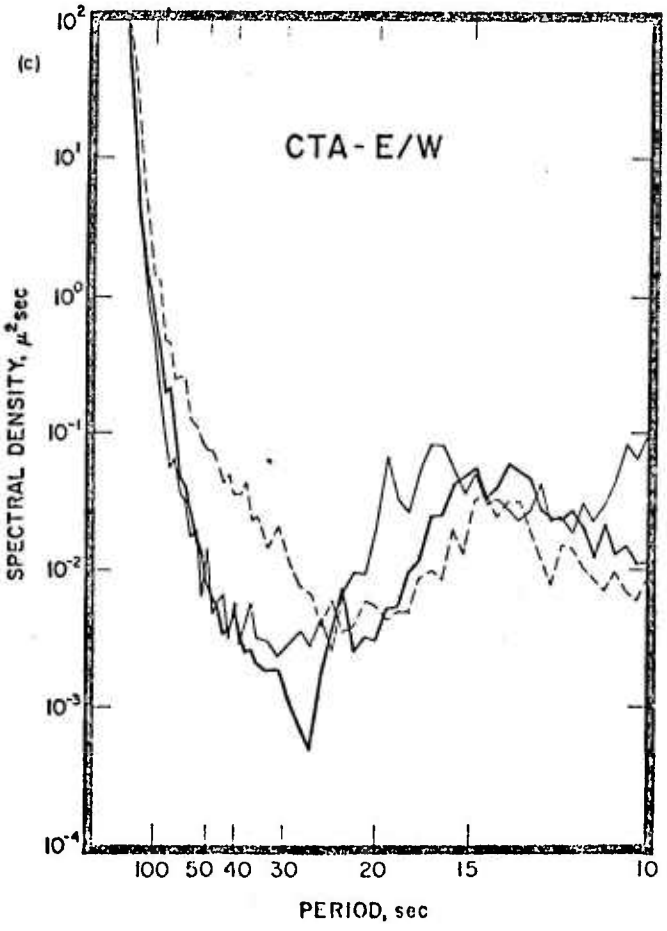


Figure 4.

Earth noise power spectra for the vertical seismograph (a), the north/south (b) and the east/west (c) horizental seismographs at CTA. The same legend is used in the three figures.

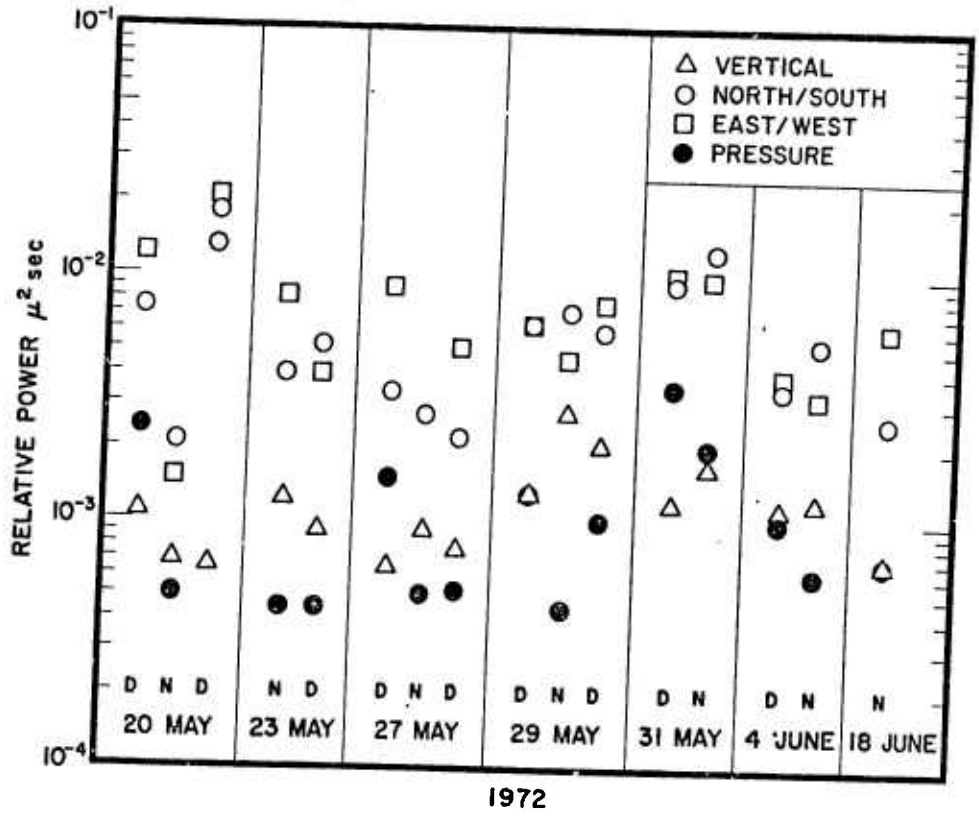


Figure 5. 40 sec levels of earth noise power for the three seismic components and of microbarographic power at CTA on seven days in 1972. The 40 sec levels of earth noise power are plotted at their absolute values; the 40 sec level of microbaregraphic power is plotted relatively. D refers to daylight hours about 03:00 → 15:00 local time, N to nighttime hours about 17:00 → 02:00 local time. Note that the level of vertical earth noise varies over a narrow band while the levels of horizontal earth noise varies over a much wider band. The levels of microbarometric noise and horizontal earth noise are reasonably well correlated.

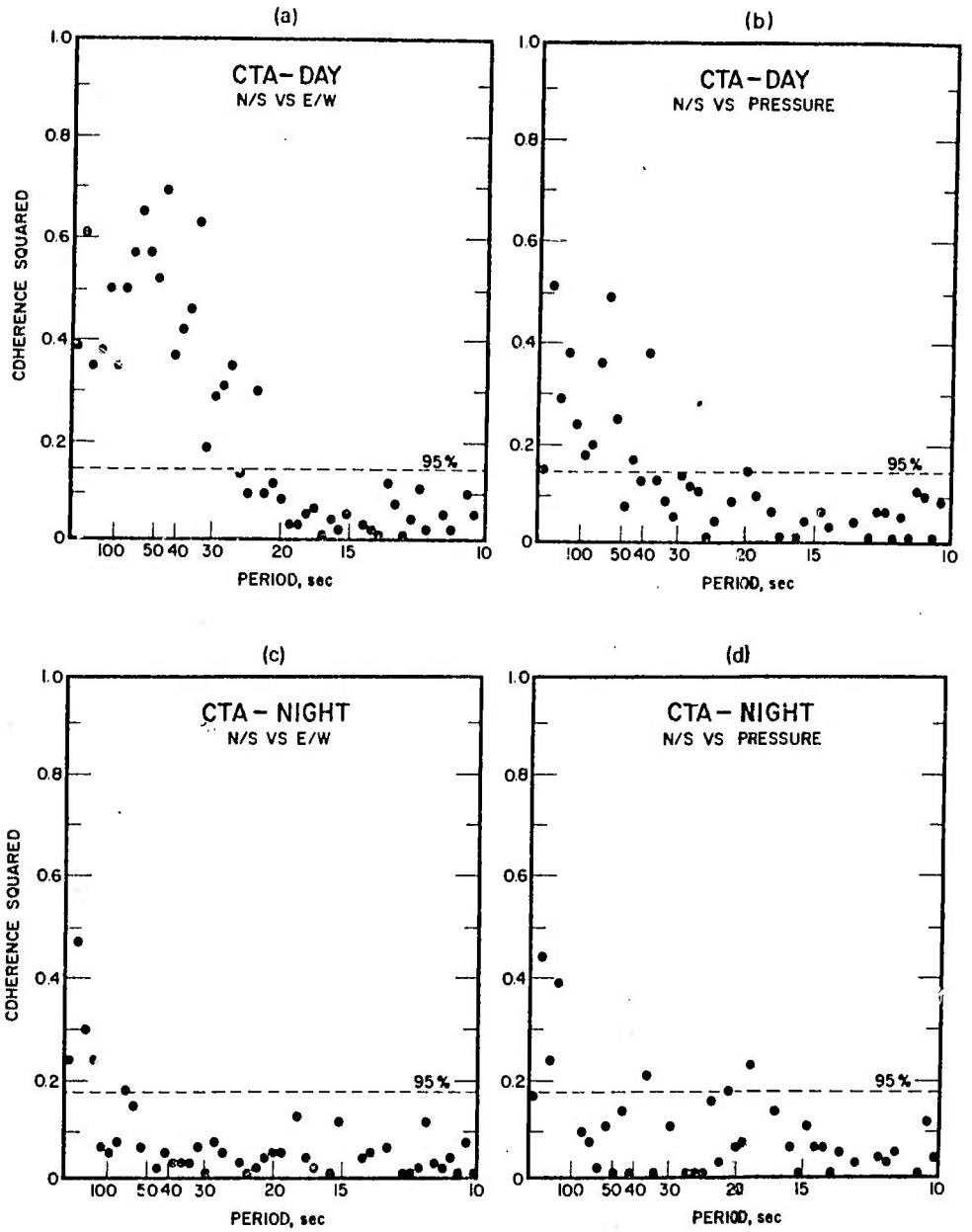


Figure 6. Squared coherence measurements between the two horizontal seismographs (a) and between the north/south horizontal seismograph and microbarograph (b) at CTA with data samples taken during daylight hours. Coherence squared measurements between the two horizontal seismographs (c) and between the north/south horizontal seismograph and the microbarograph (d) at CTA with data samples taken during nighttime hours. Note that the squared coherence between the daylight measurements are significant from about 30 to 100 sec but that the nighttime measurements display significantly less coherence.

zontal seismographs. During nighttime hours the correlation between the earth noise and atmospheric pressure variations is significant only at periods greater than about 170 sec (Figure 6d); a similar observation is the case for the correlation of the earth noise recorded by the horizontal seismographs (Figure 6c). A comparison of the power spectra of horizontal earth noise from both nighttime and daylight time intervals and of atmospheric pressure variations provides evidence that the majority of the difference between nighttime and daylight power spectra of horizontal noise may be attributed to differences in atmospheric pressure. Table 1 shows that if the difference between nighttime and the daylight microbarographic power spectrum is added to the nighttime power spectrum of horizontal earth noise, one obtains a very good approximation to the daylight power spectrum of earth noise. This is shown by the near equality of the spectral differences, day-night, of the horizontal earth noise and spectral difference of the microbarographic noise. Note that vertical spectral differences are not nearly equal to pressure differences.

Sources of Earth Noise Recorded by Vertical Seismographs at all HGLP Sites and by Horizontal Seismographs at Deep Sites. Savino et al. (1972) showed that for the HGLP instrumentation at OGD, the level of earth noise at 40 sec was approximately 20 db above the instrumental noise levels. At 200 sec this separation has decreased to about 8 db, so we have limited this study to periods less than 200 sec. Figures 7a and b are shown to emphasize the similarity of the power spectra of vertical earth noise for ten of the HGLP seismograph stations.

Despite observations that the earth noise recorded by the vertical seismograph does not change appreciably with depth and that the long-period end of power spectra of the earth noise recorded by the vertical seismographs rises at a rate of 12 to 14 db/octave and despite the data from numerous power spectra and cross-spectra and the information obtained from calculations with the Sorrells model, still only general comments can be made about the source of earth noise recorded by vertical seismographs. First if the seismograph vault is located on competent bedrock, the vertical earth noise is independent of ordinary atmospheric pressure variations. Second as reported by Savino et al. (1972) the window in the earth noise spectra near 40 sec may be a "transition between the swell-generated microseisms at periods less than 30 sec and non-propagating seismic ground motion of atmospheric origin at periods greater than 40 sec". A recent paper by Sorrells and Douze (1974) provides additional insight into a possible atmospheric source for the long-period earth noise recorded by a vertical seismograph. They report on an experiment conducted near Dallas, Texas, using a microbarograph array and single vertical seismograph and microbarograph pair approximately 65 km from the array. On 28 Feb. 1972 the microbarograph array detected a very low level signal with oscillations of 20-100 sec period from the northwest travelling with an acoustic velocity of about 330 m/sec. The signal was probably a Mountain Associated Wave (MAW) train (Larson et al., 1971) generated in the coastal ranges of British Columbia. For the time period during which the acoustic signal was being recorded by the microbarograph

TABLE 1.

DIFFERENCE, IN db, BETWEEN POWER ESTIMATES

TAKEN AT NIGHT AND DURING THE DAY

| INSTRUMENT | 20 | 40 | 60 | 80 | 100 seconds |
|---|---|---|---|---|---|
| Pressure | 1.4 | 8.1 | 10.4 | 12.4 | 10.6 |
| North/South | 2.1 | 9.3 | 11.7 | 9.0 | 7.9 |
| East/West | 3.7 | 11.4 | 15.0 | 12.6 | 12.8 |
| Vertical | 4.0 | 0.1 | 2.3 | 0.9 | 3.0 |

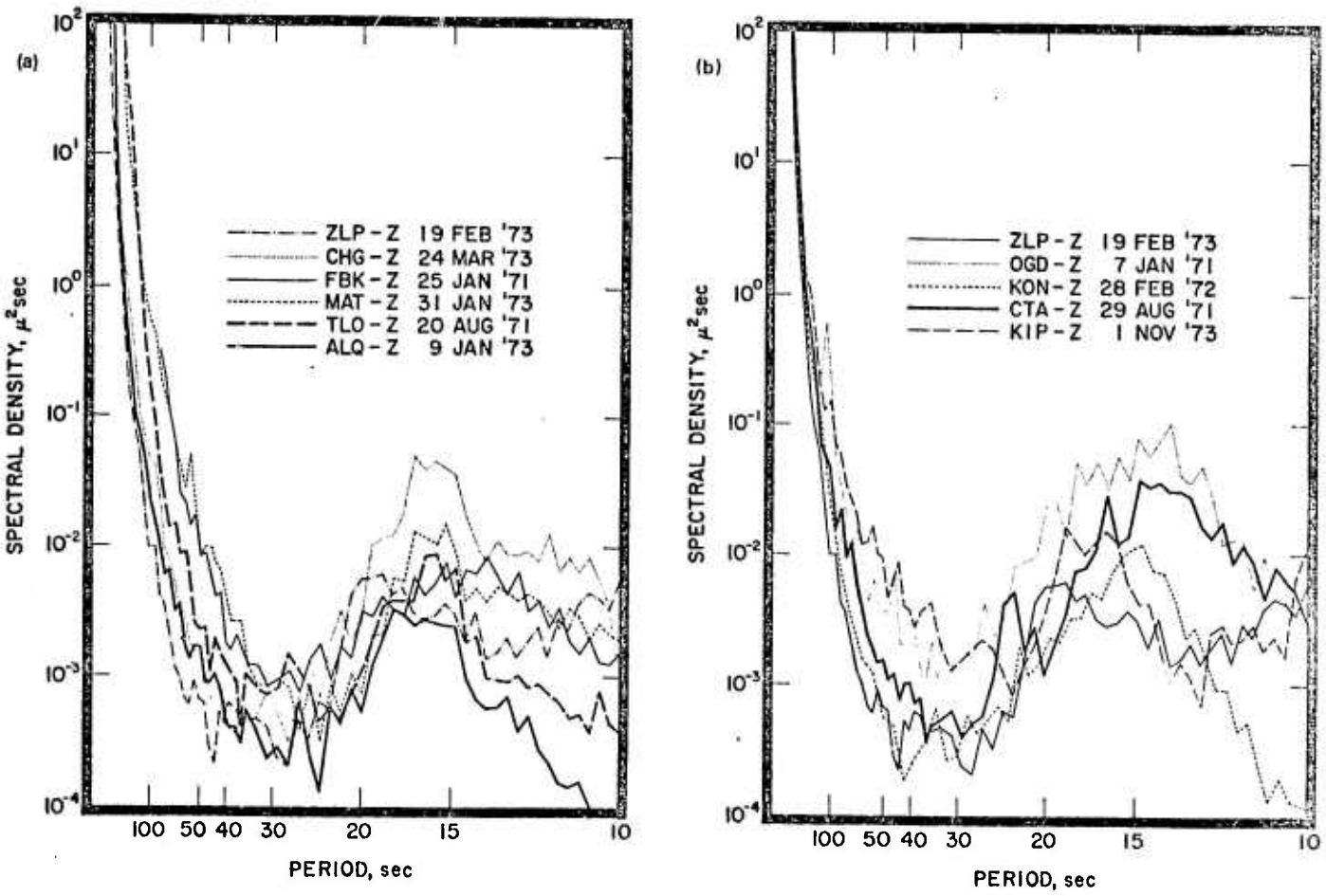


Figure 7. A set of composite earth noise spectra for the vertical seismographs at 10 HGLP stations, a and b. Note ZLP - Z is repeated as a reference.

array, the signal from the vertical seismograph was found to correlate with the signal from the single microbarograph adjacent to the seismograph. A very important factor in this observation is that a condition of near zero-velocity winds existed in the vicinity at the microbarograph; the microbarometric noise generated by the local wind would have masked the MAW-type acoustic waves recorded by the single microbarograph. Unfortunately, this single case does not provide sufficient data to establish MAW waves as a constant source of the observed long-period earth noise recorded by vertical seismographs, but it does provide additional impetus to continue a study at OGD of the atmosphere as a possible source of long-period earth noise.

Herron et al. (1969) studied the microbarographic noise spectrum using a large array (250 km) with OGD within the array. The pressure spectra rose at about 12 db/octave toward the long-period end beginning at about 150 sec. The pressure spectra displayed the same seasonal variation that Savino et al. (1972) observed in the earth noise spectra from OGD. These two observations provide an indication that the two noise spectra, pressure and earth, are related but not necessarily as cause and effect.

The most helpful data in determining the source of earth noise recorded by horizontal seismographs at the deep HGLP stations and at the shallow and intermediate-depth stations during quiet intervals are the shape and absolute level of the power spectra and the near-equality of the noise level observed on both vertical and horizontal seismographs.

If power spectra of the earth noise recorded by the horizontal seismographs are compared with power spectra of the earth noise recorded by the vertical seismograph for ZLP (Figure 2), it is apparent that during the quietest intervals the shapes and absolute levels of the power spectra are quite similar. The same observation can be made for the other deep stations. This may be taken as an indication that earth noise recorded by the horizontal and the vertical seismographs are generated by the same source. Cross-spectra have been calculated between the earth noise recorded by the vertical and that recorded by the horizontal seismographs and the correlation was not significant at the 95% confidence limits. Thus, if there is a single source for the two noise types, it must be "random" in effect or produce only very low level coherence among the three components.

Finally, the 12 to 16 db/octave rise in the earth noise spectra is a very strong indicator that the principal source of earth noise recorded on both vertical and horizontal seismographs is not earthquake coda. Two opposing theories on earthquake radiation (Archambeau, 1968 and Brune, 1970) state that earthquake spectra are either falling off toward the long-period end or are constant at long-periods, but not rising at 12 to 16 db/octave. Thus, earthquake coda are probably eliminated as a principal source of earth noise recorded on vertical seismographs.

Conclusions. The recent installation of 11 high-gain seismograph stations on a world-wide basis and the variety of geologic and tectonic settings of these stations provide an important new data base on the nature of long-period earth noise. Examination of several years of

seismograms and analysis of digital data recorded at these sites lead to the following conclusions concerning the spectral characteristics and temporal behavior of long-period earth noise:

1. In general, earth noise spectra calculated for all the sites exhibit a minimum level in the period range 25 to 45 seconds.

2. The level of earth noise recorded by vertical seismographs is apparently independent of local meteorological conditions. The low noise levels achieved at the shallow sites are a result of the sites being located on competent rock formations and having rigid environmental control.

3. The level of earth noise recorded by horizontal seismographs is dependent upon the depth of overburden. At the shallow sites (depth of overburden < 100 m) the earth noise levels exhibit a general diurnal cycle. This cycle appears to be caused by local tilting of the ground associated with daily variations of atmospheric turbulence.

4. The special HGLP-type horizontal seismographs on the 103 and 153 m level of the Ogdensburg Deep Mine Observatory and the other HGLP horizontal seismographs show that the earth noise (tilts) associated with atmospheric turbulence are attenuated, in general, to about 10% of the surface level by about 150 m in competent rock formations, i.e., noise level at 150 m depth is 10% of the noise level on the surface.

5. The source of the long-period earth noise recorded by the vertical seismographs and by the horizontal seismographs at the deep station is probably of atmospheric origin. This aspect of the problem of earth noise source will receive further investigation.

## 2. Attenuation of Long-Period Earth Noise with Depth

A vertical array of long-period seismographs was constructed in the Ogdensburg Deep Mine Observatory to measure the attenuation of earth noise with periods near 40 sec over the depth range 0 to 543 m. Using a model derived by Sorrells (1971) to predict ground motions produced by a slow-moving, plane-wave pressure disturbance, we calculated the expected attenuation with depth. According to the model this attenuation is dependent upon the velocity at which the pressure disturbance is propagating. The observed attenuations correspond to velocities that are consistent with the velocities of atmospheric phenomena that have previously been reported to produce ground motions recorded by long-period seismographs.

The tilt motions recorded by horizontal seismographs appear to be generated by low velocity (<5 to 10 m/s) turbulence in the atmospheric boundary layer immediately above the surface of the earth. These motions are significantly attenuated by about 100 to 150 m of competent overburden (Figure 8). The vertical and horizontal displacements and tilt motions produced by atmospheric disturbances travelling at acoustic velocities (about 300 m/s) are not significantly attenuated by 500 m of overburden. Thus, the signal-to-noise ratio on horizontal seismographs can be significantly improved by burial at depth of several

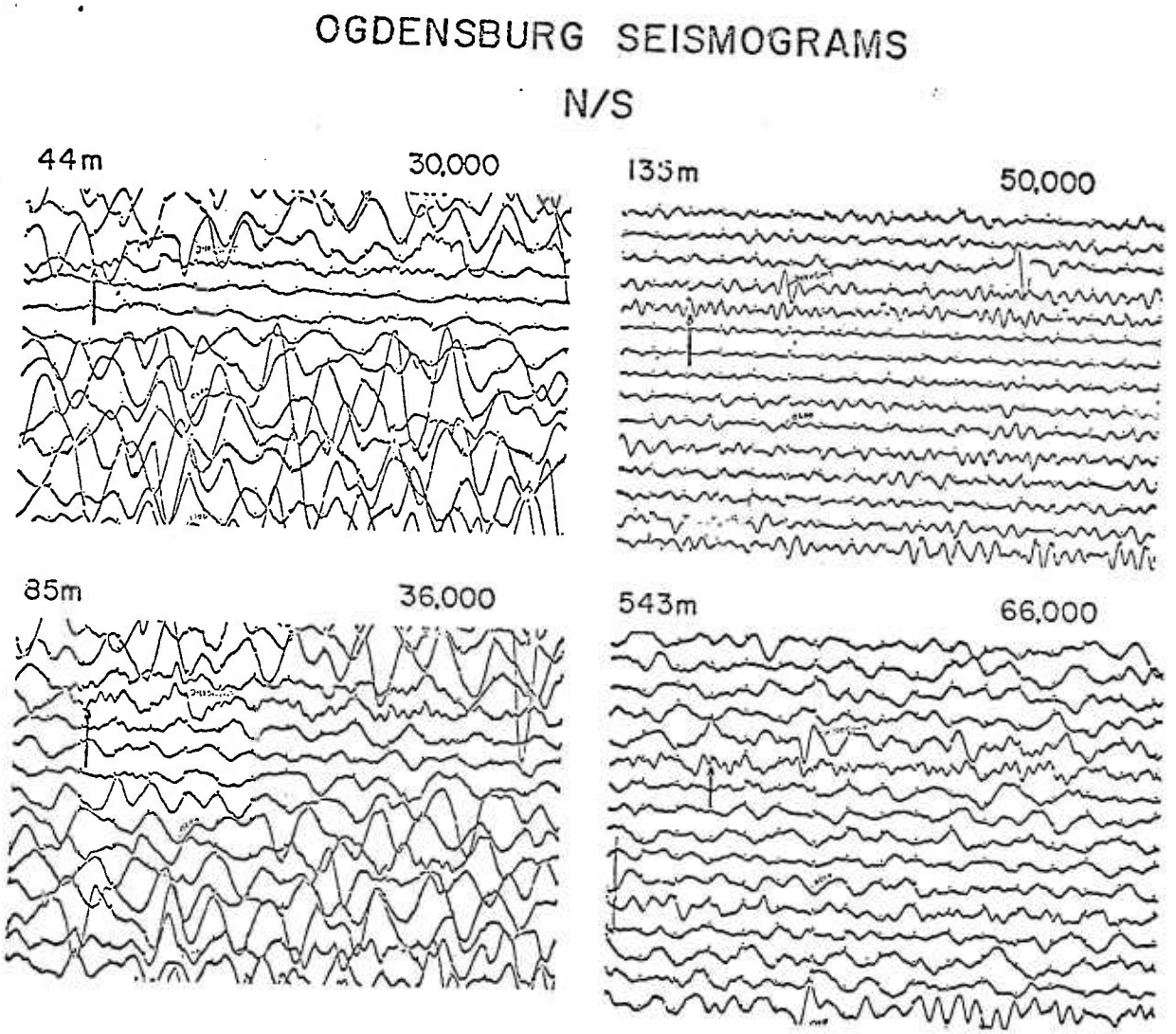


Figure 8. Attenuation of horizontal earth noise with depth. Four simultaneous horizontal-component seismograms from an array of VLP type instruments installed on four different levels of the New Jersey Zinc Mine at Ogdensburg, New Jersey show a significant increase in signal to noise level as depth of burial increases. Note also increase in magnification with depth.

hundred meters which removes the major portion of the tilt noise associated with low velocity winds, but the signal-to-noise on the vertical and horizontal seismographs cannot be further improved without going to impractical depths of burial (more than two or three km).

## 3. Detection of Air Waves

Acoustic-gravity waves from an event on 14 October 1970, presumed to be a Chinese atmospheric explosion, were observed on high-gain vertical and horizontal component seismograms written at three different locations in the world (Figure 9). Reliable group velocity data for the atmosphere over propagation paths as long as 97° (10,800 km) were obtained for the period range of 30 seconds to 375 seconds. These data are in agreement with theoretical dispersion curves that are based on the COSPAR-model atmosphere with the effects of winds included. Seismic body and surface waves from this atmospheric event were also recorded at the three stations and were used to determine an epicenter.

There are two important points about the recordings of the acoustic gravity waves on the seismograms in Figure 9. First, because of the very long-period character of these waves, it should be quite simple to detect their presence in the midst of shorter-period surface waves from a seismic event by applying low-pass filtering. Second, these waves are recorded with a very high signal-to-noise ratio in the period range 60-100 sec. A part of the seismic background is included on each seismogram for comparison. These acoustic gravity waves were also recorded on microbarograms at stations near Palisades, New York, approximately 50 km SSE of Ogdensburg and at College, Alaska. Comparison of the microbarograms with the high-gain seismograms from OGD and FBK shows that the infrasonic waves with periods between 60 and 100 sec were recorded with higher signal-to-noise ratios on the seismograms than on the microbarograms. At periods of >100 sec the response of the high-gain seismographs falls off rapidly with period ($\sim$18 db/octave), and thus the recorded amplitude of the infrasonic waves is reduced at these longer periods.

On 14 April 1971, slow speed gravity waves from another pressure disturbance of meteorological origin were observed with periods between 240 seconds and 360 seconds on seismograms at Ogdensburg, New Jersey (Figure 10). The seismic recordings of the acoustic-gravity and the slow speed gravity waves are attributed to ground motion produced by surface loading and not to direct pressure effects on the instruments. The observed displacements and tilts from both events are in agreement with those predicted by static loading theory. At the Ogdensburg station, the rock layer above the instruments (543 m) acts as a wave-length filter to suppress wind noise of short wavelength and to enhance signals from long wave-length (coherent) disturbances in the atmosphere.

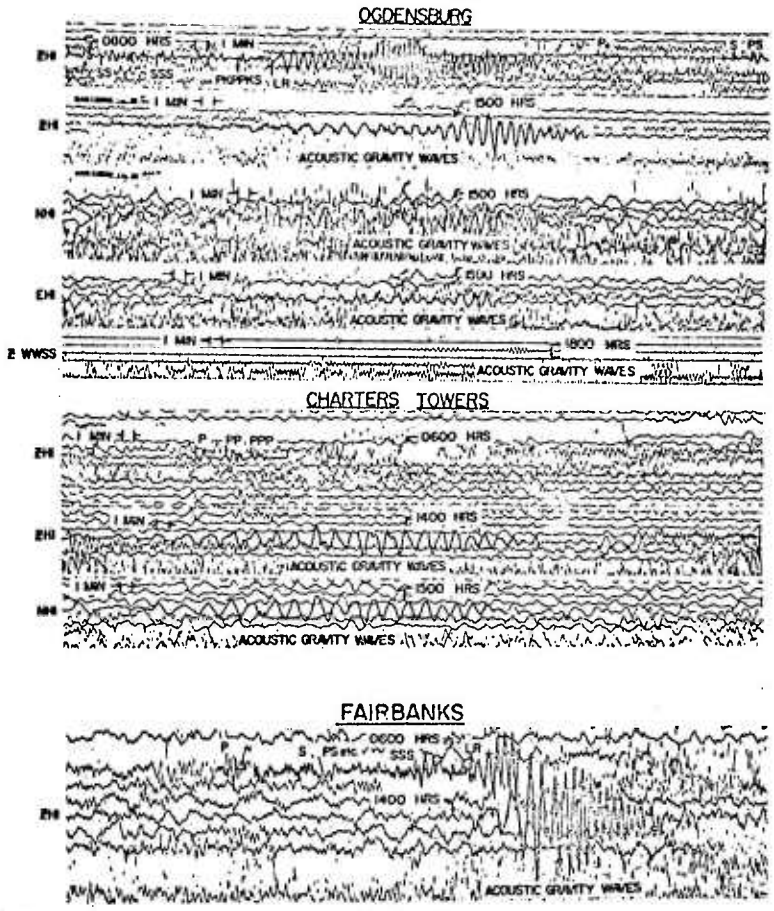


Fig. 9. Seismograms showing long-period body phases, surface waves, and acoustic gravity waves for the presumed Chinese atmospheric explosion of October 14, 1970, from the vertical (ZHI) and horizontal (NHI, EHI) component high-gain seismographs at Ogdensburg ($\Delta$ = 10,798 km), Charters Towers ($\Delta$ = 8939 km), and Fairbanks ($\Delta$ = 7276 km) and from the long-period vertical WWSSN component seismometer at Ogdensburg. The time base on all seismograms is 1 hr/line.

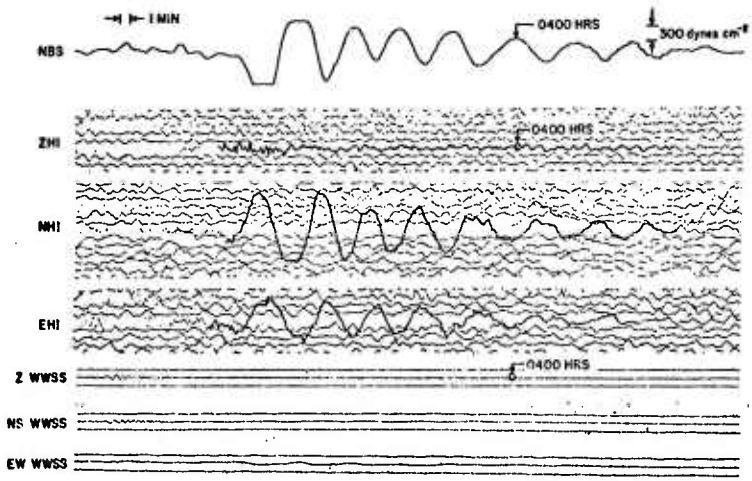


Fig. 10. Microbarogram and three-component high-gain and WWSSN seismograms for a local atmospheric event on April 14, 1971, recorded in the mine observatory at OGD. The scale given for the microbarogram refers to the sensitivity of the microbarograph at periods between about 60 and 280 sec. On either side of this period range the response of the microbarograph falls off at about 6 db/octave.

## 4. Very-Long-Period Microseisms

The double frequency (DF) microseisms (period of about 6 to 8 sec) are surface waves generated by the non-linear interaction of trains of oppositely travelling ocean waves (Longuet-Higgins, 1950; Hasselmann, 1963). The primary frequency (PF) microseisms (period of about 12 to 17 sec) have been described by Haubrich and McCamy (1969) as surface wave noise generated by ocean waves near the coast, particularly in the vicinity of large storms. The sources for transient background noise phenomena are not as well understood. Oliver (1962) studied a rare 27 sec PF microseism storm, Haubrich and McCamy found DF surface waves generated in the wake of an unusually swift tropical storm far at sea, and Savino and Rynn (1972) studied the ground displacements produced by slow-speed gravity waves from a pressure disturbance of meteorological origin.

Recently, Murphy and McCamy made an extraordinary observation of 35 to 40 sec Rayleigh wave microseisms at the Kongsberg (KON) high-gain, long-period seismograph station. The Kongsberg station is well situated in southern Norway to record DF and PF microseisms generated by gales in the North Atlantic. During the International Seismic Month (20 Feb. - 19 March, 1972), the power spectra was calculated for nearly every day. For the days during which severe DF and PF microseisms were absent, the power spectra display a pronounced minimum between about 30 and 45 sec, but for four days during which severe DF and PF microseism storms were present the minimum was less pronounced and the level was raised about 10 db.

The coherence between the vertical and north/south (N/S) components during one of the four severe DF and PF microseism storms is significant for the majority of periods less than 40 sec; and, although the phase spectrum between the same two components does not show the 90° or 270° relation between them as expected for Rayleigh waves, there is a trend in the data toward 90° as the period decreases. The departure of the phase spectrum from 90° to 270° does not rule out Rayleigh wave type ground for at least two reasons. The phase spectrum has not been corrected for a possible changing phase shift between the two components and an accurate phase spectrum is expected only for those periods with near-unity coherence. (If the Rayleigh wave motion is broad beam or combined with significant Love wave motion, unity coherence is not expected.)

The signal from the three components for a portion of the time sample was passed through a 6-pole, low-pass, Butterworth filter with a corner period of 35 sec. A plot of these traces shows three things: reasonably good correlation between the vertical and N/S traces, the peaks of about 40 sec signal on the vertical trace lead the peaks on the N/S trace, and the vertical and E/W traces correlate far less well.

There was no significant coherence between the vertical and E/W components for this same period of time. These three observations of significant coherence between vertical and N/S component, an approximately 90° phase shift between vertical and N/S component with vertical leading, and no significant coherence between vertical

and E/W components, are good indicators that what we have observed are 35 to 40 sec Rayleigh wave microseisms with retrograde motion coming from a source north of KON. A check of the surface weather charts for the northern hemisphere shows that there is a large low pressure system north of KON for the proper time interval, that is, allowing for ocean wave propagation from the storm to the coast line. It is likely that this storm is the source of the ocean wave energy responsible for the DF and PF microseism storm. The possibility that the observed signal was the coda of a large earthquake was eliminated by checking the list of earthquakes for the International Seismic Month and by searching for similar noise at the same time at the Toledo and Ogdensburg HGLP stations. No large earthquake is listed near the time of the microseism storms, and the signals were not observed as far away as TOL or OGD.

## B. MAGNITUDE THRESHOLDS OF THE HGLP STATIONS

### 1. Detection Capabilities of 8 High-Gain Stations versus the WWSSN

A detailed investigation of seismograms from eight high-gain stations for the time period 8 September 1971 to 15 September 1971 (inclusive) was undertaken to compare the number of earthquakes recorded at these eight stations with the number reported by NOAA in the monthly listings of the PDE. While long-period surface waves, of both the Rayleigh and Love type, are the primary type of seismic wave that the high-gain detection results are based on, events are reported in the PDE listings on the basis of the recording of short-period body phases at at least a few of the stations of the WWSSN. The results are shown in Figure 11 in the form of a histogram.

The numbers inside the hatched (lower) sections in Figure 11 refer to the number of earthquakes reported in the PDE and observed at the station indicated; the solid sections refer to the number masked at a particular station; and the stipled sections to the number of unreported events observed at a particular high-gain station. Of the 103 reported events (the hatched section of the column designated WWSSN), 79 were recorded on one or more of the seismograms from the eight stations as indicated in the column adjacent to that for the WWSSN. Of the remaining 24 reported earthquakes, 15 were definitely not observed at any of the high-gain stations. Six of these 15 events were assigned focal depths greater than 100 km, 6 others were not assigned any body-wave magnitudes, and the remaining 3 were assigned magnitudes less than 4.0 and occurred at distances greater than 25 to 30° from the closest high-gain station.

The number of events observed on the combined high-gain seismograms but unreported by PDE is 73. This gives a total of 152 events observed during this time period or approximately 20 per day. During this same time period short-period body phases from 197 events were reported in the bulletin from the Large Aperture Seismic Array (LASA) in Montana. Note that we cannot compare these numbers with one from the PDE program since many of the earthquakes that are detected at

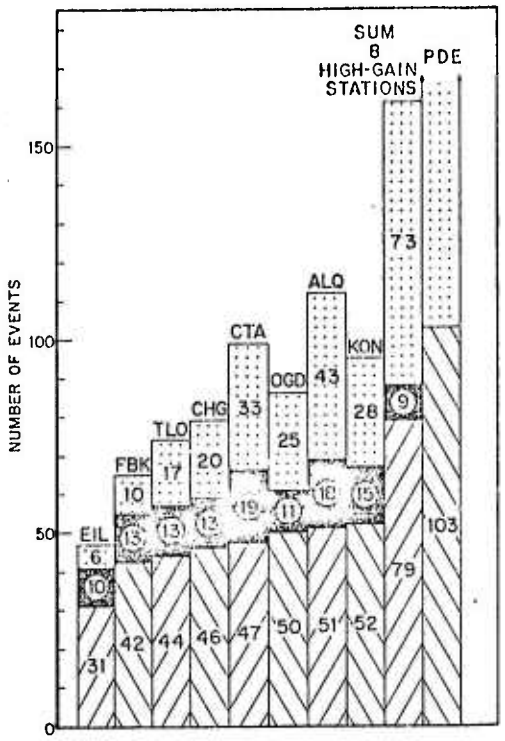


FIG. 11. Histogram comparing the detection capabilities of each of the high-gain stations with that of the PDE.

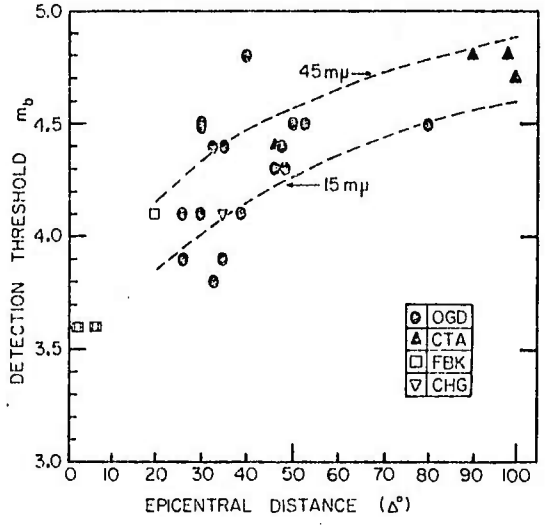


FIG. 13. Plot of $m_b$ vs. epicentral distance for the more reliably determined values. The dashed curves represent expected thresholds for high (45 mμ) and low (15 mμ) background noise conditions.

a few isolated stations of the WWSSN are not located and thus go unreported. For this reason the number of unreported, but detected, events for the WWSSN is left open-ended. To be sure it is in excess of the total number observed on the high-gain seismograms and probably also the number reported in the LASA bulletin.

The number of NOAA-reported earthquakes with surface wave trains masked by the coda of larger events is 9 for the combined seismograms from all eight high-gain stations. This number is not greatly different from the numbers of masked events at any one station and points up one of the most important problems with the detection of long-period surface waves from shallow events. While more sophisticated analysis techniques than the visual one employed in this study would probably identify some of these masked events, it remains to be seen how successful these techniques will be in routine practice. Notice, however, that the number of surface waves (79 + 73 = 153) detected on the combined high-gain seismograms is about double the number detected by a single high-gain station.

## 2. Regional Magnitude Threshold

Seismograms from the stations at OGD, CTA, FBK, EIL and CHG were analysed for more than 1000 shallow focus ($h<60$ km) earthquakes reported in the PDE to assess the dependence of the detection capability for long-period surface waves of a particular station on the geographical locations and epicentral distances of earthquakes. Figure 12 shows the surface wave detection thresholds with respect to a particular station for 59 seismically active areas. The thresholds are expressed in terms of body-wave magnitude, $m_b$, as determined by NOAA (PDE) with the exception of western North America (exclusive of Alaska) where Evernden's (1967) formulas for $m_b$ were used. Magnitudes of earthquakes outside western North America are not likely to change significantly if Evernden's formulas are used rather than those of NOAA since the percentage of stations at distances less than 18° is nearly always small. The values of $m_b$ indicated on the map represent the smallest magnitude earthquakes from which surface waves were consistently observed at one of the high-gain stations during the particular time-period of this study. When a value of the magnitude threshold is given in Figure 12 for a particular region, it means that all earthquakes reported in the PDE (the data base) for that region with magnitudes equal to or greater than this threshold value generated observable surface waves.

The less than symbol (<) indicates that we were only able to determine an upper limit for the value of the magnitude threshold in a particular region because of the inadequate number of small magnitude earthquakes reported in the PDE for that region. Improved detection and reporting of short-period body phases would allow the determination of more accurate surface-wave thresholds for events in these regions.

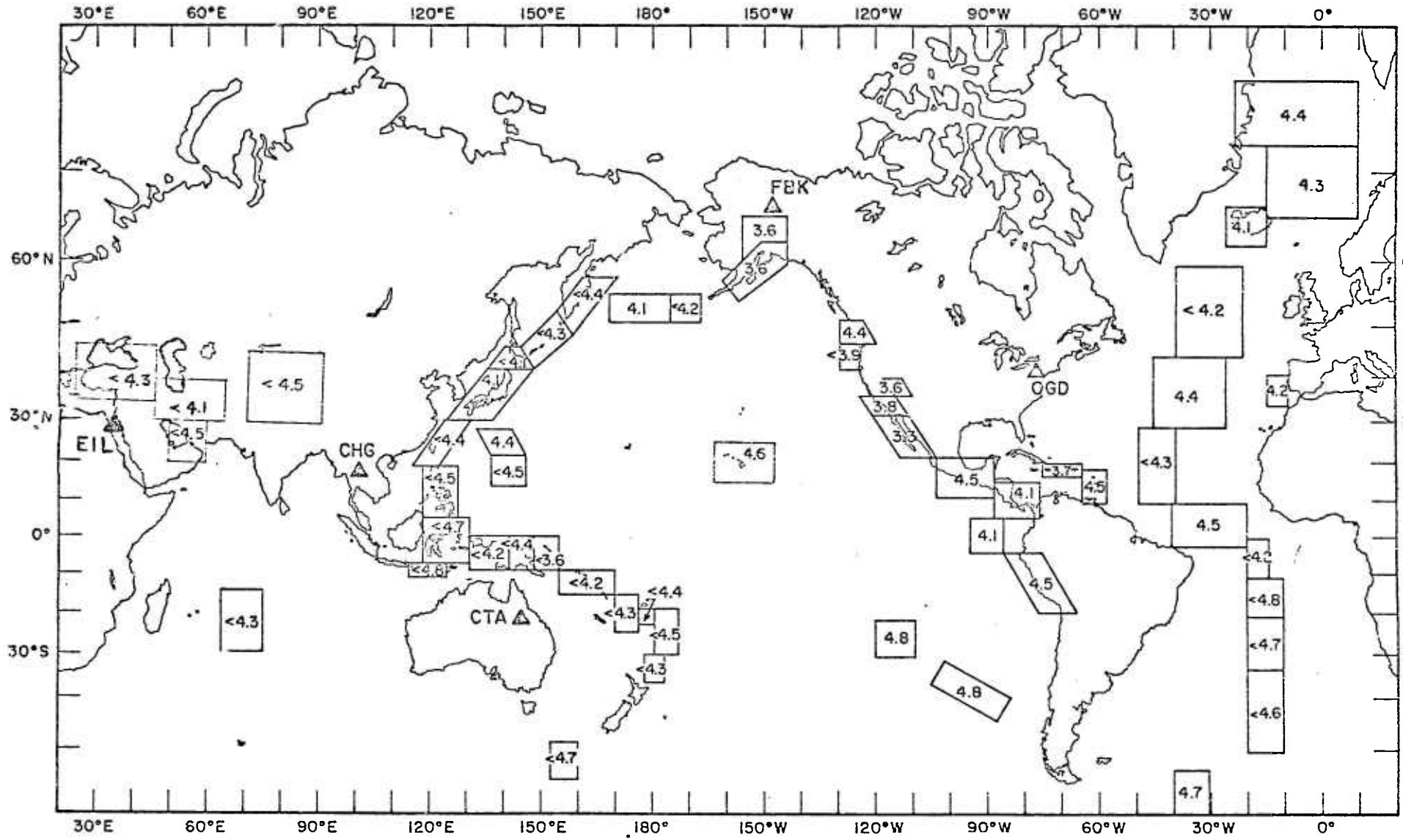


FIG. 12 Map of the world showing values of the detection thresholds in terms of $m_b$ for surface waves from shallow focus earthquakes listed in the PDE. These threshold values were determined with data from the five high-gain stations indicated by the solid triangles.

The regions determined using OGD data include the North and South Atlantic Ocean, the Caribbean, South America, western United States, and Vancouver Island. Six months of data from FBK were used to determine thresholds in Alaska, the Aleutians, and the Kuriles-Kamchatka regions; four months of CHG data for Hokkaido, Honshu, Ryukyu and the mid-Indian Rise; six months of EIL data for Tibet, Iran, and Turkey; and six months of CTA data for the remaining regions of the western Pacific and Easter Island. It is important to note that in many of these regions, surface waves from earthquakes with $m_b$ values as much as 0.75 units less than the threshold values indicated in Figure 12 were observed.

The better determined threshold values given in Figure 12 are plotted in Figure 13 as a function of epicentral distance. In the distance range 20° to 25° , the detection threshold for long-period surface waves is approximately $m_b$ = 4.1 (PDE). The dashed curves in Figure 13 represent the expected thresholds under relatively high and low noise conditions. These curves were computed using the magnitude relationships described by Gutenberg (1945). The noise level of 15 mμ represents a record amplitude of 1 mm at 20 s which is about the lowest limit for visual analysis under ideal conditions. While these thresholds for surface waves with periods of 20-40 s represent an improvement over existing seismograph systems, the various digital enhancement techniques that can be applied to the data from the high-gain systems should result in a further lowering of the threshold values.

## 3. Detection Capabilities of the HGLP Stations During International Seismic Month

Recently the Seismic Discrimination Group at Lincoln Laboratory compiled a special listing of the occurrence of as many events as possible for the time period 20 February 1972 through 19 March 1972. Hereafter this special listing and the above 1 month time period will be referred to as the International Seismic Month (ISM). The final version of the ISM listing contains 996 entries identified on the basis of short-period body waves recorded on the various arrays (LASA, NORSAR, ALPA); the Canadian, Swedish, and United Kingdom seismograph networks; and the WWSSN stations. The ISM listing serves as an excellent data base to be used in the determination of approximate detection thresholds of the high-gain stations. The results discussed in this study were based on a preliminary listing containing 840 events.

Figure 14 shows the percentage of reported events above the plotted magnitude for which surface waves were observed at one or more of the high-gain stations. Only shallow (h<100 km) events which had two or more stations reporting a magnitude were used in this comparison. Note that surface waves were observed for 90% of the reported events of $m_b$ 4.6 or greater. Half of the 10% of these events not observed were the result of masking by the coda of earlier larger events. Significantly, the largest single event

not in coda for which surface waves were not observed was of $m_b$ 4.8, and one additional event of $m_b$ 4.7 was also missed. All the remaining events not in coda for which surface waves were not observed were of $m_b$ 4.6 or less.

Two other important observations that are not obvious from Figure 14 come from the analysis involved in the preparation of this figure. They are the following:

1. Approximately 10% of the events observed at the deep stations EIL, OGD, and KON were observed on the basis of long-period Love waves only. The reason for restricting this statement to the deep stations is that the horizontal component seismographs at these sites operate with peak magnifications equivalent to those of the vertical component systems. In addition the low noise levels on the horizontal component seismograms from these three stations do not undergo any obvious diurnal variations as do the horizontal noise levels at the other shallower sites (Murphy et al., 1972; Savino et al., 1972a and b).

2. Surface waves with periods between 30 and 50 seconds were recorded from more than 90% of the 465 observed events. This percentage is greater than that for the number of events for which surface waves with periods near 20 seconds were observed.

The histogram in Figure 15a gives an idea of how the VLP stations as single stations (e.g., CTA column) fared in terms of the ISM listing (column headed ISM). The numbers inside the lightly stippled sections of each of the VLP columns refer to the number of world-wide earthquakes reported in the ISM that excited surface waves of either the Rayleigh or Love type with periods between about 15 to 60 seconds and which were observed at that particular (see column heading) VLP station. Note that about 55% (465) of the 840 reported events were detected at at least one of the VLP stations, more than twice as many than the number detected at any one site. While it is not entirely evident from this figure, the combination of the five stations EIL, FBK, CTA, ALQ, and KON are responsible for more than 90% of the 465 observed events.

The varying heights of the individual VLP columns in Figure 15a reflect the amount of time no records were available from the different stations. For all the stations except KIP and CHG, these times were mainly due to analog record changing intervals; digital data are available for these times. The KIP station became operational on 7 March 1972, more than half way through the ISM time period. This accounts for the relatively small number (281) of events considered. Approximately 7 days of recordings from CHG were not available.

The numbers in the open sections of the VLP columns and the additional numbers in the hatched sections of the TLO, OGD, and KON columns designate the numbers of reported events that were

TABLE 2.

90% surface wave detection thresholds ($m_b$)

| | 20° to 30° | 30° to 40° | 80° to 100° |
|---|---|---|---|
| CTA | | 4.0 | 4.9 |
| EIL | | 4.2 | 4.9 |
| ALQ | ~ 4.2 | | 4.4 |
| KON | 4.0 | | 4.5 |
| TLO | ~ 4.5 | | 4.7 |

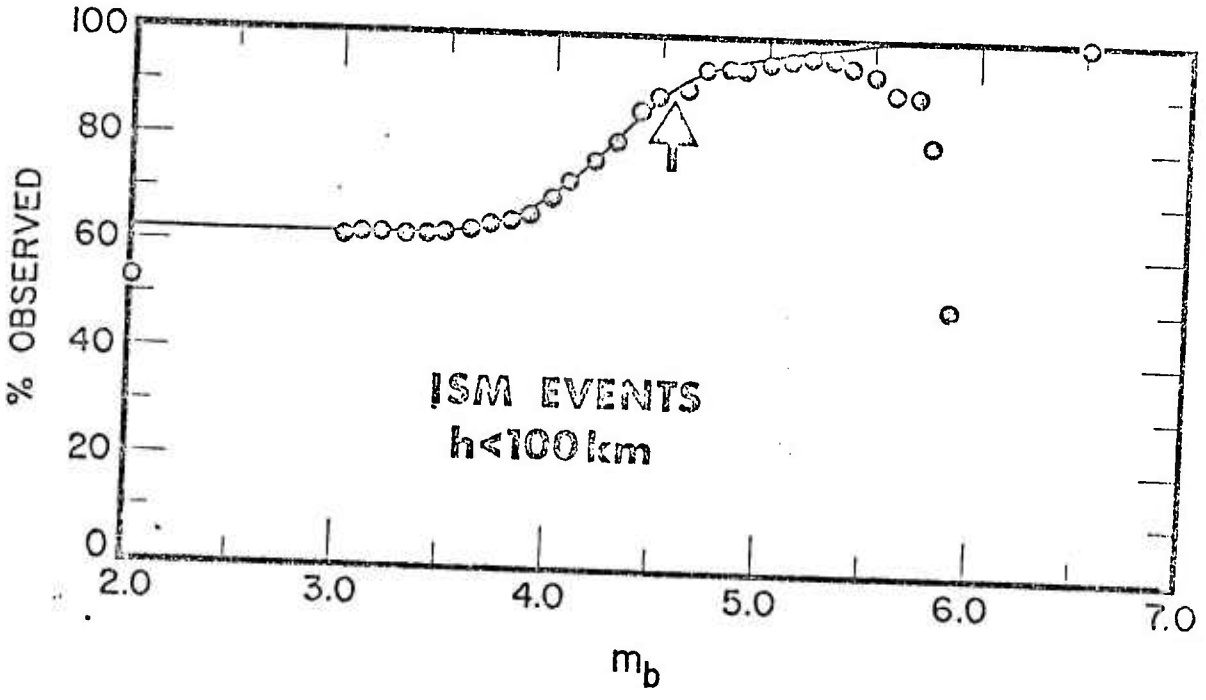


Figure 14. Percentage of shallow events during the International Seismic Month for which surface waves were detected at one or more high-gain long-period seismic station.

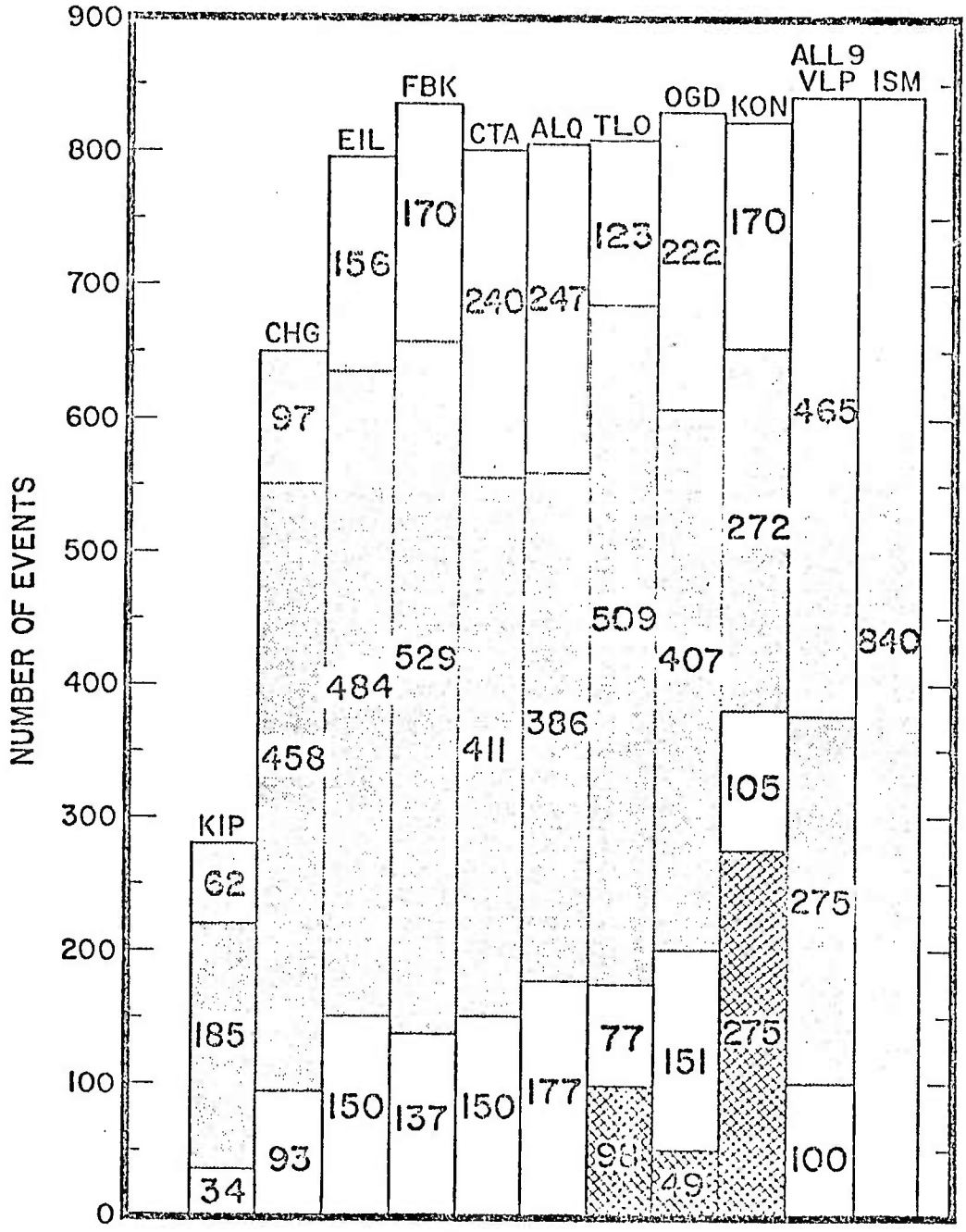


Figure 15. a) Histogram comparing the detection capabilities of each of the VLP stations with the ISM.

b) Histogram comparing the detection capabilities of the nine VLP stations during a quiet 48 hour time interval (left-hand side) and a 48 hour time interval during which masking is severe (right-hand side).

c) Histogram comparing the detection capabilities of the nine VLP stations for events of either shallow focal depths ($h \leq 50$km) or $h > 50$km.

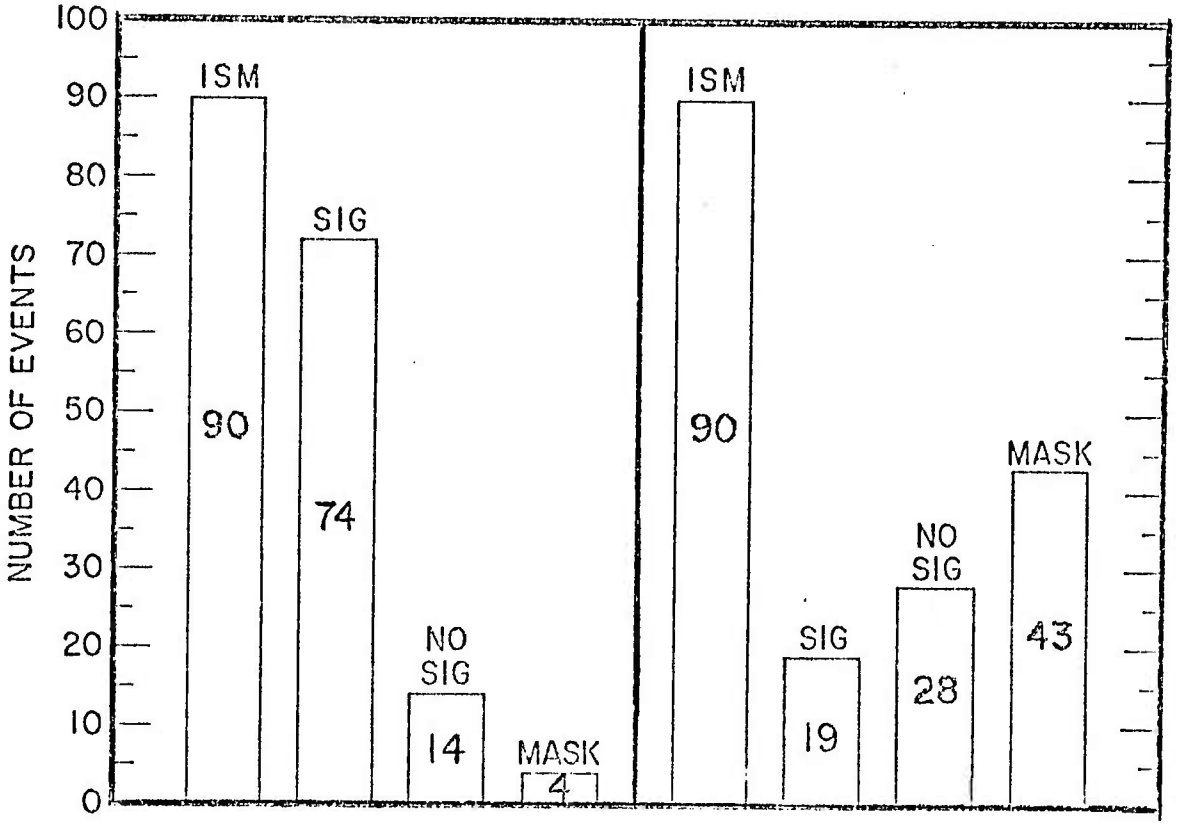


Figure 15b

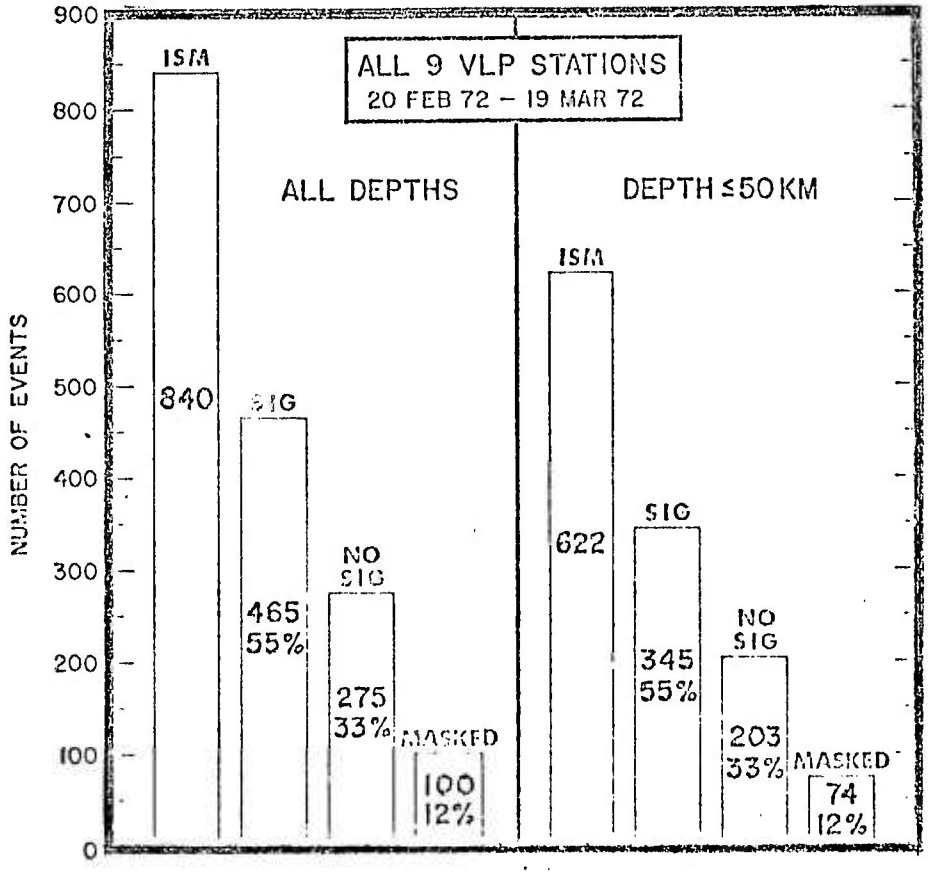


Figure 15c

masked by either body waves and/or surface waves (coda) from a larger event (open sections) or masked by large amplitude microseism storms comprised of surface waves with periods near 16 to 20 seconds. Note that the severity of the masking problem ranges from 46% of the events considered at KON to 16.4% at FBK. The effect of combining all nine VLP stations is to reduce the number of masked events to 100 out of 840 or 12%. Actually the number or percentage of masked events based on all the VLP stations (12% here) for the most part will not be significantly smaller than the smallest number or percentage obtained at some one station (e.g., FBK 137). This is a result of the well developed, and widely recorded, coda of surface waves associated with shallow events of magnitudes greater than 5.0 to 5.5. During the ISM month two events with magnitudes greater than 6.0 occurred and were responsible for 50 of the 100 events masked.

During the winter months in the northern hemisphere, and especially in the north Atlantic, microseism storms of both the double frequency (7 to 9 sec) and primary frequency type (15 to 18 sec) are particularly common. For instance microseism storms that occurred during the ISM month accounted for as much as 33% of the visual masking problem at KON. In this regard, however, it is interesting to note, although well understood (Haubrich and McCamy, 1969; Hasselmann, 1963), that while several double frequency storms were observed on the low-gain or standard seismograms from KIP, because of the structure of the Hawaiian Islands (the absence of a sloping shelf) there were no observable primary frequency storms. Thus, in terms of masking, the long-period (T>15 sec) detection thresholds determined during the ISM at this mid-ocean station depended only on the coda problem discussed above.

As both microseism storms and the occurrence of large magnitude earthquakes are transitory phenomena it is of interest to compare the performance of the nine VLP stations during a time interval when both of these masking sources are active with a time interval when both sources are absent. In Figure 15b, the performance of the VLP stations during two 48 hour time periods within the ISM month are compared. The time interval on the left-hand side corresponds to the absence of large earthquakes and microseisms while that on the right-hand side corresponds to the dominance of one or both sources. Note the drastic change in the detection capabilities from 72 out of 90 (80%) during quiet times to 19 out of 90 (21%) reported events being observed when masking is severe. The corresponding percentage change in the number of masked events is tenfold. While masking is obviously a problem with the VLP systems, it must again be pointed out that all the results presented so far are based only on visual analysis of analog recordings. It is to be expected that some rather simple filtering techniques (low-pass, band-pass) and the more sophisticated techniques of matched filtering and polarization filtering (Choy and McCamy, 1973) that can be applied to the digitally recorded data at these sites will improve (lower) the detection thresholds, especially during recording intervals that are visually dominated by either microseisms or interfering events.

A final point to be considered concerning the results in Figure 15a is the question as to how do the VLP stations fare detection-wise when only shallow (here taken as h<50 km) events are considered. Figure 15c gives the answer to this question. Comparing the right-hand (all depths) and left-hand side of this figure, we find that the percentages of events observed (SIG), not observed (NO SIG), and masked do not change when the ISM listing is screened for deeper events. To some extent this result is surprising. One possible explanation, however, is that depths greater than normal (h>33 km) were in many instances not assigned to the very small magnitude events. This is not unexpected since the very small events were probably poorly recorded making proper depth determination extremely difficult.

To study detection thresholds as a function of distance, all those events listed in the ISM as having a focal depth of 50 km or less, and assigned a body-wave magnitude ($m_b$), were considered. In Table 2 values of the 90% detection thresholds in two different $10^o$ distance ranges are given in terms of $m_b$ for 5 of the VLP stations. Because of insufficient data at CTA and EIL in the $20^o$ to $30^o$ distance range threshold values were instead determined in the $30^o$ to $40^o$ range at these two staions. From Table 2 we find that mean values of the 90% detection thresholds for surface waves range from $m_b$ = 4.2 at $30^o$ to about $m_b$ = 4.7 at $90^o$. It should be noted again that these threshold values are based on visual analysis of seismograms and that the filtering techniques described by Choy and McCamy (1973) should lower these values by at least 0.2 $m_b$ units.

## C. DISCRIMINATION BETWEEN EARTHQUAKES AND PRESUMED UNDERGROUND EXPLOSIONS IN CENTRAL ASIA

Previous results from a high-gain station on the $M_s$-$m_b$ discriminant between earthquakes and underground explosions in different regions of the world were reported by Molnar et al. (1969), Evernden et al. (1971) and Savino et al. (1971). These earlier studies were based on data recorded at OGD. In this section we will concentrate on results from one of the more recent stations, that at Eilat, Israel. This station is approximately $30^o$ from presumed Russian underground explosions and exhibits a lower detection threshold for surface waves from these presumed explosions and earthquakes in the same general region than the stations at Chiang Mai, Thailand (CHG); Kongsberg, Norway (KON); and Toledo, Spain (TLO).

In Figure 16, peak-to-peak amplitudes of Rayleigh waves recorded at Eilat with periods near 20 sec (left-hand plot) and 40 sec (right-hand plot) from earthquakes in the Kirzig-Sinkiang-Tadzhik-Tibet region (closed circles) and presumed Russian explosions (open circles) are plotted as a function of $m_b$ (NOAA). The ordinate on the 20 sec plot describes the Ms scale for these events as indicated by the numbers and arrows. Although the data are limited there are two rather important points about Figure 16. Firstly, the earthquake and explosions populations are completely separated even though the

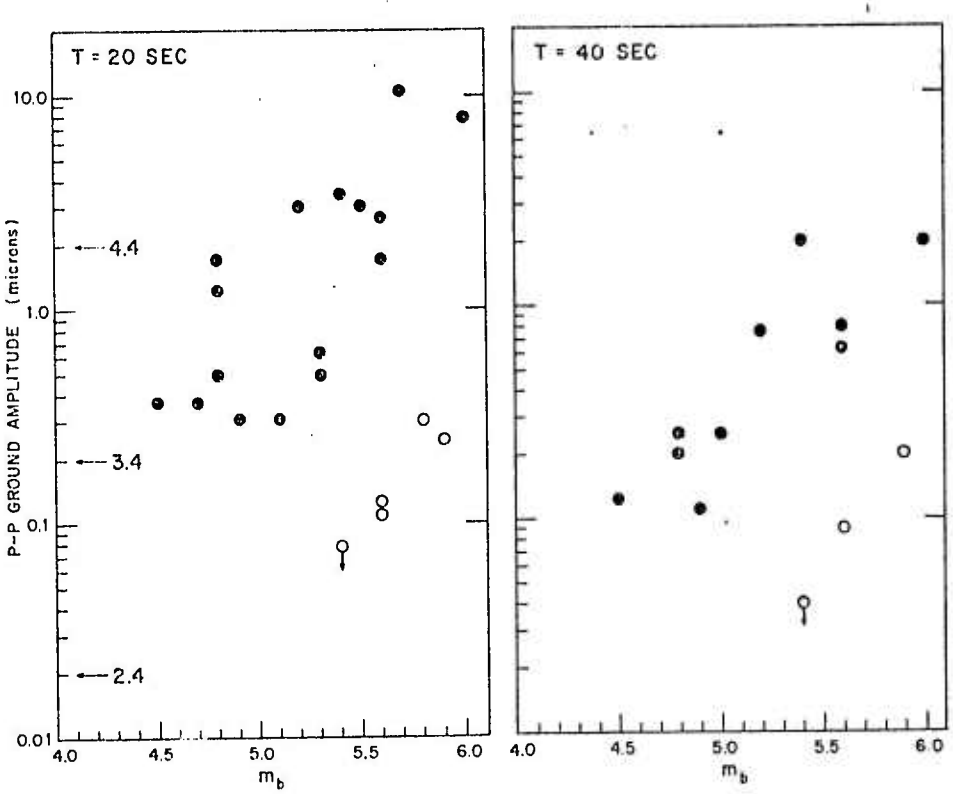


FIG. 16. $M_s$--$m_b$ at 20 and 40 s (Rayleigh waves) for earthquakes in the Kirgiz–Sinkiang–Tadzhik–Tibet region (closed circles) and presumed Russian explosions (open circles). All of these measurements were taken from seismograms from the station at Eilat, Israel. Note the pronounced separation of the two populations.

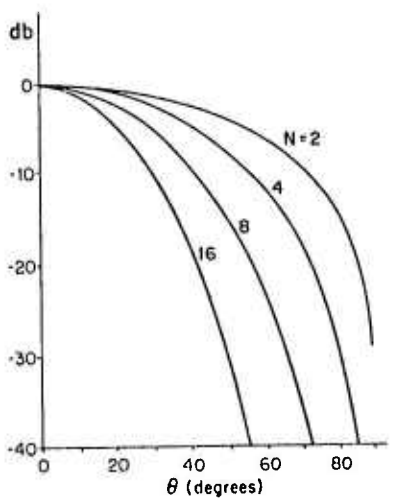


Fig. 17. The rejection exponent $N$ of the filter transfer function determines the amount of rejection of signals whose angle $\theta$ arrives incorrectly polarized or off azimuth.

measurements are restricted to a single station. Secondly, the two populations do not show any sign of convergence at the low magnitudes, although it must be remembered that the NOAA (PDE) reports do not include most events from this area smaller than about $m_b$ = 4.5 to 4.8. This latter result is similar to that found at OGD for earthquakes and explosions in the western United States, the Aleutians, and the Novaya Zemlya region (Molnar et al., 1969; Savino et al., 1971).

## D. ENHANCEMENT OF LONG-PERIOD SIGNALS BY TIME-VARYING ADAPTIVE FILTERS

As detection thresholds are lowered, the performance of any network becomes limited not only by ambient noise but also by the masking of small events by larger ones. That is, if the effect of background noise is reduced, the only competition against detecting a desired signal is the presence of other signals. To help overcome this limitation on the performance of the high-gain stations, we applied time-varying adaptive filters to the seismograms from individual stations. A signal-to-noise enhancement of more than 6 db (0.3 magnitude unit) was attained for Rayleigh waves from small events. Love waves may play an increasingly important role in discriminating between seismic sources. Hence we also investigated the effectiveness of using time-varying adaptive filters for extracting Love waves masked by the coda of a larger events.

### 1. Filters

The filter transfer functions are shaped to pass frequency bands where the signal-to-noise ratio is momentarily high. We define a high signal-to-noise ratio in two different ways: by the apparent polarization of particle motion and by the apparent azimuth of arrival. The first criterion is used in the 'polarization' filter. The relative phase angle between the vertical and horizontal motion $\theta(f)$ is inspected as a function of frequency, and then the amplitude response of the filter is shaped to pass either body waves ($\theta(f) = 0$ or $\pi$) or Rayleigh waves ($\theta(f) = \pm \pi/2$). The second criterion is used in the 'azimuthal' filter. Here the apparent direction of arrival of Love waves on the two horizontal instruments is inspected as a function of frequency. The amplitude response of the filter is shaped to pass energy in the frequency bands where the apparent signal is near the azimuth of the suspected event.

We briefly outline the strategy of our computations. We are given two digitized seismograms $x_i$ and $y_i$ ($i = 0, 1, 2, \ldots$, in seconds). For the polarization filter, x and y are the vertical and horizontal seismograms. For the azimuthal filter they are the two horizontal seismograms. We take segments of length m and operate on them in turn. In the kth segment we take

$$\hat{x}_i^k = x_{(i+km/2)} \qquad i = 0, 1, \ldots, m-1$$

$$\hat{y}_i^k = y_{(i+km/2)}$$

We compute their Fourier transforms $\hat{X}_j$ amd $\hat{Y}_j$. For the polarization filter the phase angle $\theta_j$ is the argument of the cross spectrum

$$\theta_j = \arg \hat{X}_j \hat{Y}_j^*$$

For the azimuthal filter the angle

$$\theta_j = \alpha - \tan^{-1}(\hat{Y}_j / \hat{X}_j)$$

is the difference between the expected azimuth of arrival of the suspected event, $\alpha$, and the apparent azimuth of arrival. The filter transfer function for the kth segment is then generated: $F_j = \sin^N \theta_j$ for the Rayleigh polarization filter and the azimuth filter or $\cos^N \theta_j$ for the body wave filter. The exponent N determines the amount of rejection of the filter for frequencies whose phase angles are either incorrectly polarized or that arrive off azimuth. Figure 17 shows how power is rejected as a function of $\theta$ for the different values of N. The Fourier transforms are then multiplied by this filter to give the transforms of the filtered segments:

$$X_j' = \hat{X}_j F_j \qquad Y_j' = \hat{Y}_j F_j$$

The first half of their inverse Fourier transforms, $x_j'(k)$ and $y_j'(k)$, is combined with the last half of the preceding $(k - 1)$ segment to form the time-varying filtered output:

$$x_i'' = W_i x_i'^{(k)} + (1 - W_i) x_{(i+m/2)}'^{(k-1)} \qquad i = 0, 1, \ldots, m/2$$

$$y_i'' = W_i y_i'^{(k)} + (1 - W_i) y_{(i+m/2)}'^{(k-1)} \qquad W_i = 2i/m$$

Our experience has been that segment lengths of m = 128 sec and N = 8 usually give good results.

The filters that we call polarization and azimuth filters have been applied before with varying success at single stations to shorter-period data than we use (Archambeau and Flinn, 1965; Flinn, 1965; Sax and Mims, 1965; Simons, 1968). The major shortcoming of such filters, indeed of all filters, is that they cannot improve the signal-to-noise ratio of the data in any given frequency band. Their strength, however, is that they can objectively select and pass only those frequency bands where the signal-to-noise ratio is momentarily high. These filters, therefore, are useful not for overcoming noise, which can be done only if more than just single-station data are available, but rather for avoiding noise wherever and whenever possible.

Figure 18a shows the application of the Rayleigh wave polarization filter to an event from Venezuela recorded at Ogdensburg. Comparison of signal-to-noise ratio in the original digitized seismograms with the signal-to-noise ratio in the polarization filtered seismograms shows an unreported event also recorded at Ogdensburg. The signal-to-noise

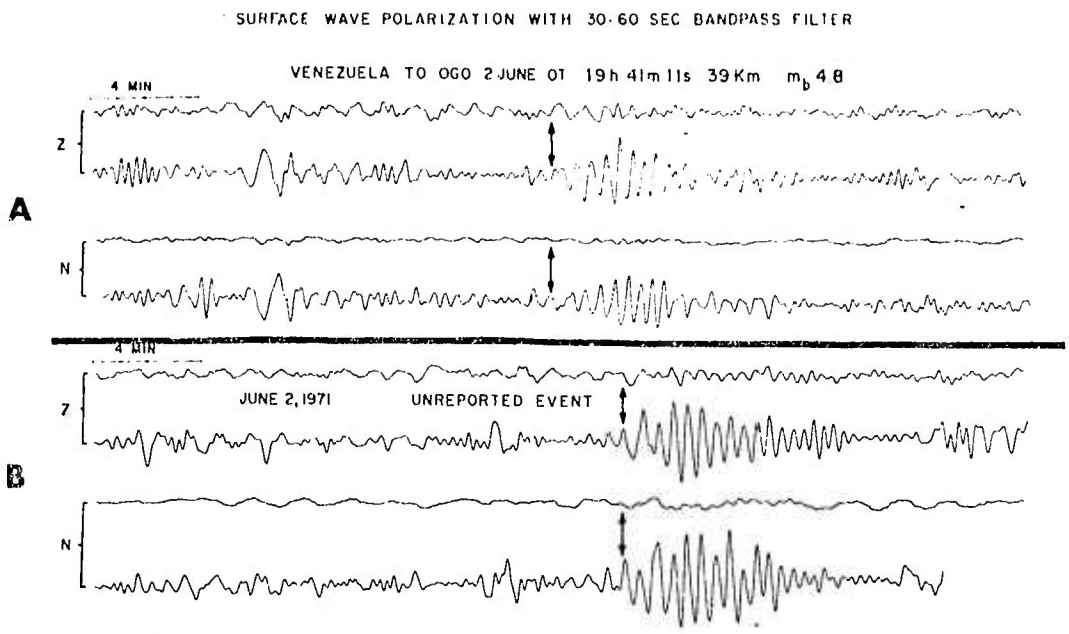


Fig. 18 (*a*) An event from Venezuela recorded at Ogdensburg. (*b*) An unreported event recorded at Ogdensburg. In both (*a*) and (*b*) the vertical and north-south components are shown. The upper seismogram of each pair is the original digitized seismogram; the lower one is the seismogram after polarization filtering.

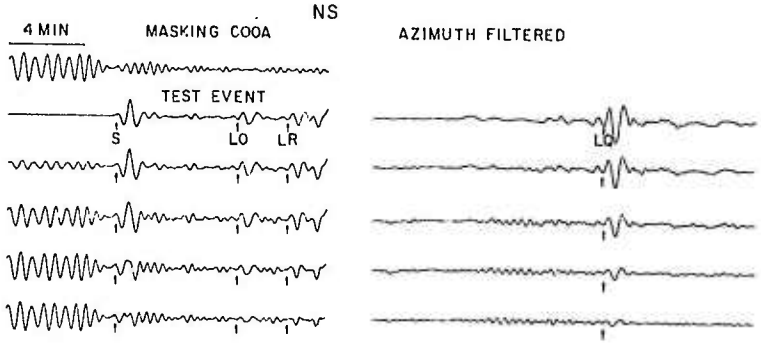


Fig. 19a. The north-south component. The first trace in the upper-left corner is the coda of an event from Iran ($m_b = 6.0$, April 12, 1971, OT 19h 03m 25.9s) recorded at Ogdensburg. Beneath it is an event from Honshu ($m_b = 5.6$, January 4, 1971, OT 21h 08m 53.4s) containing a Love wave recorded at Charters Towers. This test event is buried with decreasing energy in the coda in the succeeding seismograms. The seismograms after azimuth filtering are shown on the right-hand side.

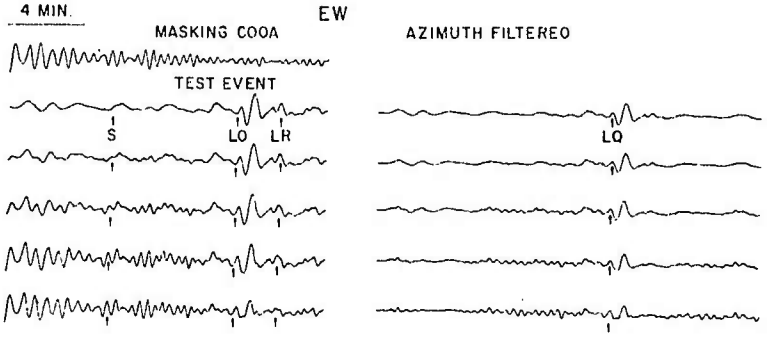


Fig. 19b The east-west component. The first trace in the upper-left corner is the coda of an event from Iran ($m_b = 6.0$, April 12, 1971, OT 19h 03m 25.9s) recorded at Ogdensburg. Beneath it is an event from Honshu ($m_b = 5.6$, January 4, 1971, OT 21h 08m 53.4s) containing a Love wave recorded at Charters Towers. This test event is buried with decreasing energy in the coda in the succeeding seismograms. The seismograms after azimuth filtering are shown on the right-hand side.

improvement in the filtered records is at least 6 db. In the case of the unreported event, knowledge of the azimuth was not required by the polarization filter.

Figure 19 shows the success of the azimuthal filter in extracting Love waves from the coda of a large event. East-west and north-south components are shown. On the left-hand side of Figures 19a and 19b are shown first the coda of a surface wave and beneath it a test event containing the Love wave that we seek to retrieve after filtering. In the succeeding seismograms, different signal-to-noise ratios are simulated by burying the test event with decreasing energy in the coda until it is no longer distinguishable. On the right-hand side of Figures 19a and 19b are the corresponding seismograms after azimuthal filtering. Retrieval of the Love wave is successful until about the last seismogram from the bottom in each case. Comparison of the largest amplitudes of the coda before and after azimuthal filtering indicates that a 14-db signal enhancement was achieved.

## 2. Discussion

Because both of time-varying filters have a built-in strategy of signal enhancement, they perform better than passive techniques such as band-pass or matched filtering. Our experience has been that the earthquake signature at periods longer than 30 sec is not really broad band and hence makes an unsatisfactory matched filter. By using either the surface wave train or the entire earthquake as a matched filter, a maximum signal-to-noise gain of 6 db is predicted by the equivalent band-width of long-period records, and even this is seldom realized in practice (Savino et al., 1972b). In some cases the result scarcely exceeds the signal-to-noise ratio of the original seismogram. Band-pass filtering often passively rejects both signal and noise.

It is clear that the success of these filters depends on the momentary content of noise. If there is frequency separation between signal and noise, the signal may be extracted even if the signal-to-noise ratio is less than 1 (Figure 18b). This is an important criterion in trying to retrieve signals from a coda (Figures 19a and 19b). Thus a long-period Rayleigh or Love train that otherwise would be above noise level may be buried by a coda yet retrievable at a single station.

If the signal and noise share the same frequency passband, the phase angle of the signal is difficult to retrieve accurately even for signal-to-noise ratios as high as 2:1. We would expect enhancement only of signals usually visible on the original record. In cases where the signal-to-noise ratio is greater than 2, the filters consistently enhance the signal at least 6 db. This would still be useful in bringing out the character and time of arrival of long-period surface waves. However, these adaptive filters will cap-

italize on any momentarily advantageous frequency bands when such are present. Hence in some cases, despite low signal-to-noise ratios and poor frequency separation, enough frequencies may be passed to yield a signal recognizable by its complex signature and dispersion. Unlike optimum filtering, no a priori knowledge of the signal and noise spectra is necessary.

## E. HIGHER MODES AS AN AID TO SEISMIC DISCRIMINATION

A paper describing the application of a surface wave magnitude scale based on the amplitude of higher-mode Rayleigh waves to the discrimination of anomalous earthquakes from underground nuclear explosions has been completed and accepted for publication in the Bulletin of the Seismological Society of America (Forsyth, 1976). By using the new higher-mode scale, $M_s^h$, several anomalous events in central Asia reported by other investigators were shown to be normal earthquakes. The conclusions based on the higher modes were confirmed in a number of cases by the observation of long-period (40 to 60 s) fundamental mode signals at the high-gain long-period station at Chiang Mai, Thailand. A relatively high ratio of higher mode to fundamental mode energy can be produced when an unusual combination of source depth and focal mechanism leads to poor excitation of the fundamental mode Rayleigh wave, in which case, the amplitude of the higher mode yields a more reliable estimate of the size of the event than the amplitude of the fundamental mode. Several anomalous events in central Asia, which are characterized by unusually low $Ms:m_b$ ratios and hence could be suspected to be nuclear explosions, are reclassified as earthquakes when the new, higher-mode scale, $M_s^h$, is employed. The focal depth and mechanism of these anomalous events apparently causes poor excitation of the fundamental mode Rayleigh wave without significantly affecting the amplitude of the higher mode. Elimination of these source related factors from traditional $Ms:m_b$ discriminants is an essential tool for reliable discrimination between earthquakes and nuclear underground tests.

In compiling surface wave data for the measurement of phase velocities along paths to the high-gain station at Chiang Mai, great variability was noticed in the amplitude of higher mode Rayleigh waves relative to the amplitude of the fundamental mode. The records from the explosions and some of the earthquakes examined were very simple and dominated by the fundamental mode. Many other records were quite complex, with the amplitude of a signal presumed to be a higher mode approaching or exceeding the amplitude of the fundamental. An experiment was designed specifically to determine whether these differences were source effects or merely due to changes in propagation path.

The effects of source variations on the seismic signal can be separated from path and receiver effects by examining several closely spaced earthquakes with different source geometries. Records from three shallow events (Figure 20 ) are used to demonstrate the pronounced changes in apparent complexity of the signals caused by relatively small variations

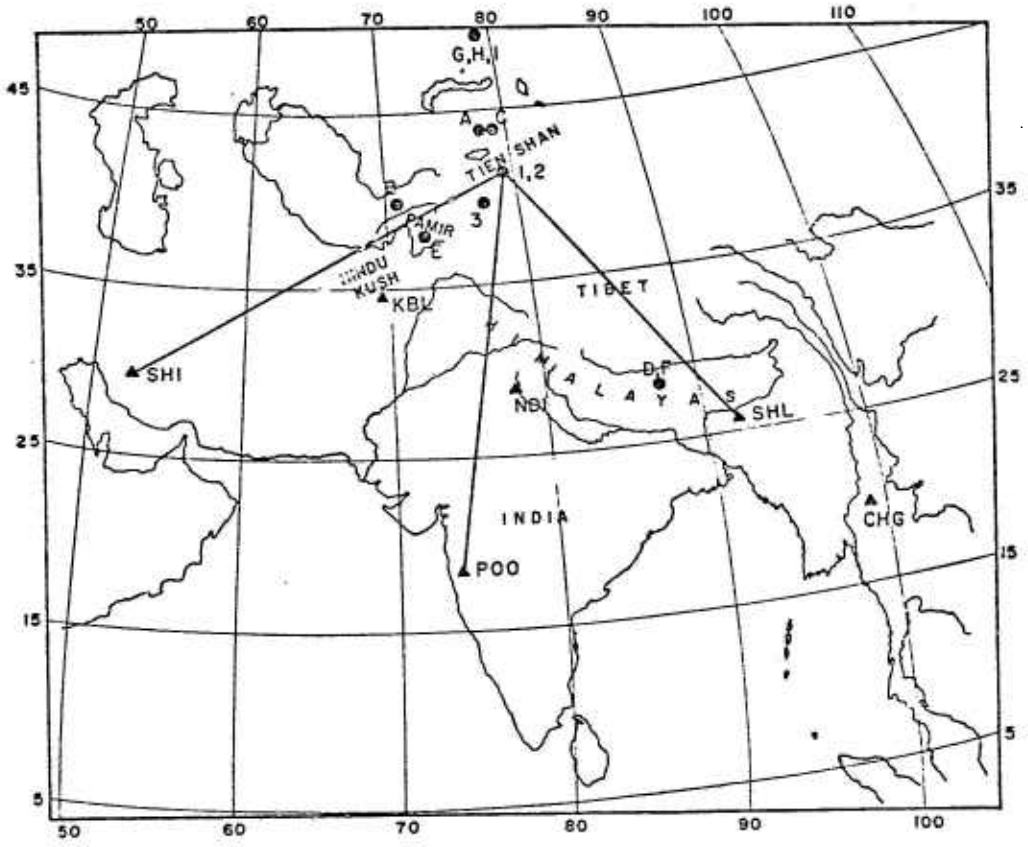


Fig. 20. Index map of source locations and WWSSN stations. Event 1 occurred at 2204 on 6/15/71, event 2 at 0834 on 5/4/65 and event 3 at 0950 on 7/29/70. Events A-I are listed in Table 3.

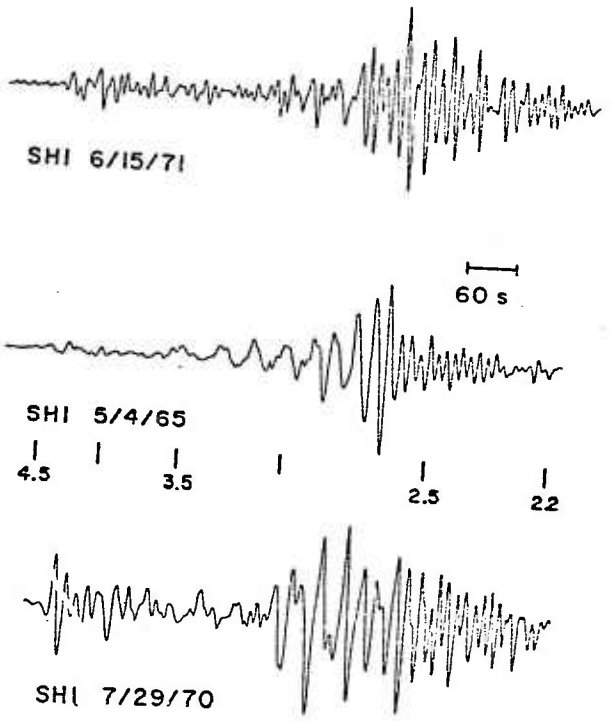


Fig. 21.

Traces of digitized seismograms observed at SHI on long-period vertical component. Each recording has been individual normalized to give constant maximum amplitude. Tick marks indicate approximate group velocity in km/s. From top to bottom, traces are events 1 through 3.

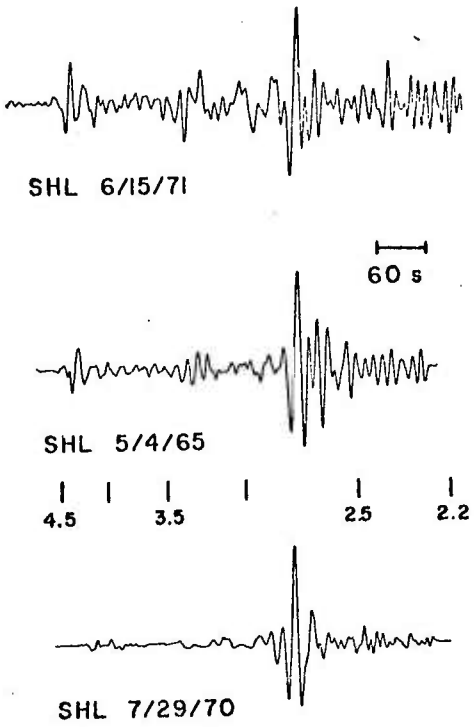


Fig. 22. Traces of digitized seismograms observed at SHL on vertical component.

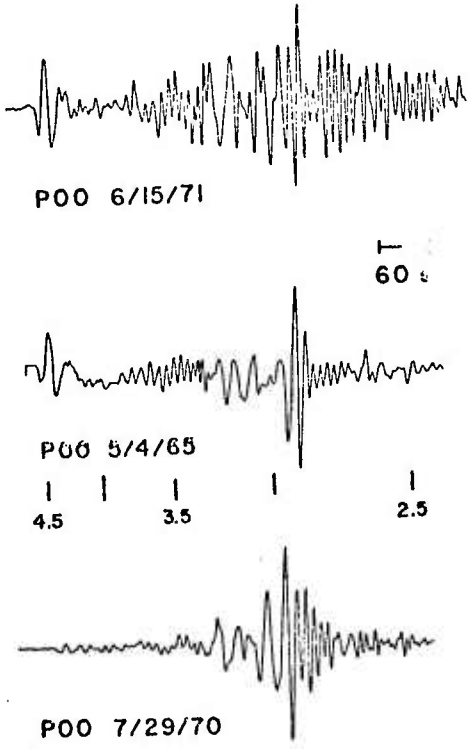


Fig. 23. Traces of digitized seismograms observed at POO on vertical component.

in source depth. Event 2 is located within about 15 km of event 1 and event 3 is approximately 150 km southwest of the first pair. Tracings of the digitized, long-period, vertical component from the three events as observed at three World-Wide Standard Seismograph Network (WWSSN) stations are shown in Figures 21, 22, and 23. The three stations, Shillong (SHL), Poona (POO) and Shiraz (SHI), cover a 120° range of azimuths and are 2,100 to 2,700 km from the epicenters. Each record has been normalized to its maximum amplitude to facilitate comparison of the waveforms.

All three records from event 1, top tracing in Figures 21, 22 and 23, are characterized by multiple arrivals of short period energy and large, rapid, amplitude fluctuations. In each figure, the S-wave is near the beginning of the record at a time equivalent to a group velocity of about 4.5 km/s. At SHI (Figure 21), there are arrivals of energy with 10s period at 3.0, 2.7, and 2.5 km/s. There are amplitude fluctuation and apparent phase shifts at several points, such as those at about 2.6 and 2.35 km/s. At SHL, (Figure 22) some apparent long-period energy arrives at about 3.0 km/s, but is overidden by the short-period oscillations which continue from the S-wave to the end of the record shown. At POO (Figure 23), there is a pronounced arrival of short-period energy at about 3.5 km/s, followed by some long period signal (~ 30s period) and high-frequency oscillations with large amplitude fluctuations.

In contrast to the "messy" records shown at the top of each figure, some of the Rayleigh waves traveling the same paths from events 2 and 3 have a markedly different, "clean" appearance. At SHI (Figure 21), the record of event 2 shows a very simple wave, normally dispersed from about 100s period at 3.6 km/s to about 8s at 2.3 km/s. The lack of apparent phase shifts and the smooth variation in amplitude do not require the path to be homogeneous between source and receiver, but it does suggest that it is unlikely that multipathing is primarily responsible for the complex appearance of the record of event 1. Since the paths are nearly identical, there must be some fundamental differences between the sources of the two records.

In Figure 24, contour plots of energy as a function of frequency and arrival time at SHL, as measured by moving window analysis (Landisman et al., 1969), show that the same dispersion curve of the fundamental mode Rayleigh wave is found for all three records despite the distinct differences in appearance. The complexity of some of the seismograms is caused by the superposition of relatively short-period energy upon the dispersed, fundamental mode arrival. Since much of this energy arrives early, it cannot be scattered or reflected fundamental mode energy. The arrival concentrated at 3.3 km/s at SHL could be interpreted as SS or a higher mode Rayleigh wave. The nature of this energy is much clearer at POO, particularly in the record of event 2, which shows a well-dispersed wave with period about 10s at 3.9 km/s to 5s at 3.4 km/s. The dispersed nature of the wave indicates that the signal must be a higher mode rather than a multiply-reflected S-wave.

There are three primary cases in which a relatively high ratio of higher mode to fundamental mode energy will be generated at the source. 1) The earthquake may be below the depth at which the fundamental mode is excited efficiently, yet still be sufficiently shallow to excite higher modes within the crustal wave guide. 2) For certain focal mechanisms, fundamental mode Rayleigh waves will be excited only weakly if the earthquake occurs at a depth corresponding to a zero crossing in displacement or stress versus depth for the wave. Zero crossings for the higher modes are generally not at the same depths, so if the amplitude of the fundamental mode is reduced by this effect, the higher modes may be undiminished. 3) Except for sources very near the surface, the azimuthal radiation pattern for higher modes may differ from the fundamental modes. At azimuths corresponding to a node in the fundamental mode radiation pattern there may appear to be a relatively large amount of higher mode energy. Although each of these three mechanisms for producing a large ratio of higher mode to fundamental mode energy is frequency dependent, they can affect a range of frequencies broad enough to significantly change the appearance of the seismogram. All three mechanisms involve reducing the amplitude of the fundamental mode rather than increasing the absolute amplitude of the higher modes. Thus, when the higher/fundamental ratio is large and the surface wave magnitude based on fundamental mode Rayleigh wave amplitudes is anomalously low compared to the body wave magnitude, a more reliable estimate of seismic moment or surface wave magnitude may be obtained from the amplitudes of the higher modes.

As one of the primary applications of an improved magnitude scale will be to aid in discrimination between earthquakes and underground explosions, the higher mode scale ($M_S^h$) is designed to be equivalent to the fundamental mode scale ($M_S$) for a near-surface focus event. The scale now commonly accepted for Asian events (Marshall and Basham, 1972; Conference of the Committee on Disarmament, 1972) is of the form

$$M_S = \log A + B'(\Delta) + P(T) \qquad (1)$$

where A is the maximum amplitude (nm) of the vertical component of ground motion in the Rayleigh wave train, T is the period of the wave of maximum amplitude, P(T) is the period correction which depends on the propagation path and $B'(\Delta)$ is a distance normalizing term that corrects for the effects of geometric spreading, scattering and absorption of the propagating surface wave. P(T) is assigned value 0.0 at the arbitrary reference period of 20s.

To equalize $M_S$ and $M_S^h$, it is necessary to know the relative amplitudes of the two modes. At the surface, the excitation function reduces to a simple form with only those terms proportional to the horizontal displacement remaining. The amplitude of the fundamental mode wave of 20s period should be approximately 7.5 times the amplitude of the first higher mode wave of 10s period for any very-near-surface focus event. The formula for $M_S^h$ should therefore be:

$$M_S^h = \log A + B'(\Delta) + \log T/T_o + \log 7.5$$

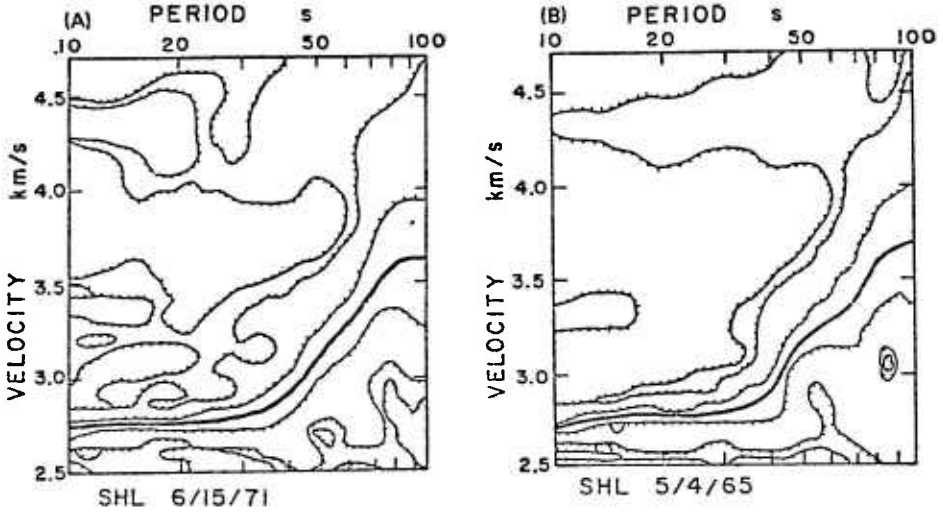


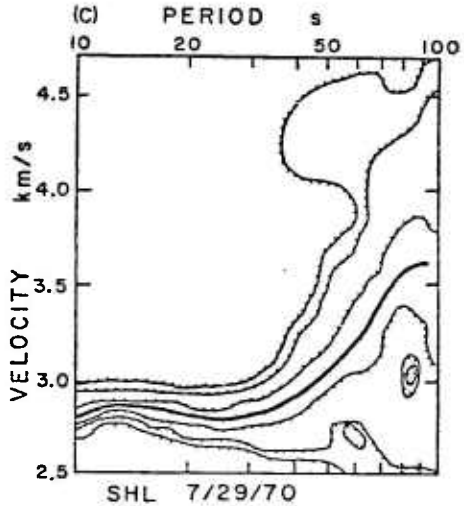


Fig. 24 a-c Moving window analysis of events 1-3 as recorded at SHL and shown in fig. 22 Each frequency is normalized independ that contours indicate equal energy levels relative to p energy at each frequency. Heavy line indicates arrival c fundamental mode. Energy arrival at about 4.4 km/s is the wave. The tick marks on contours indicate direction of de creasing energy.

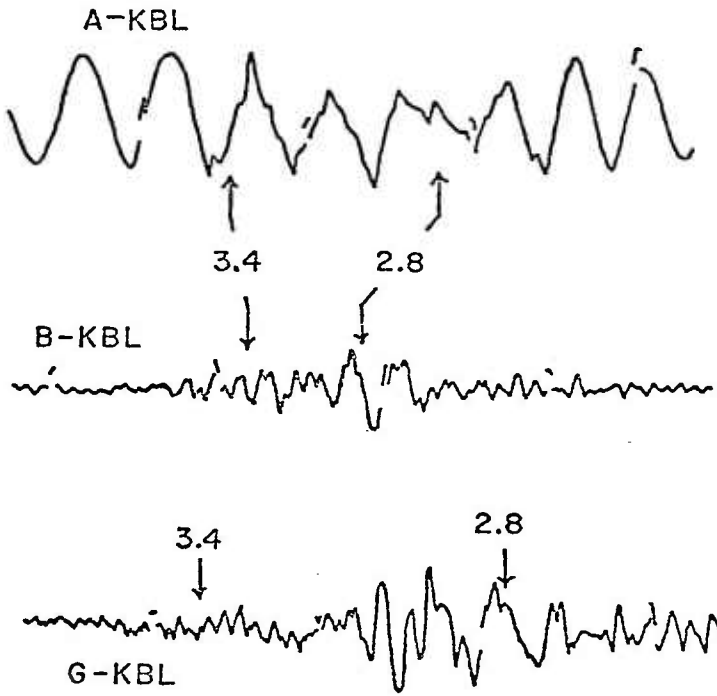


Fig. 25.

Tracings of long-period, vertical component of records at the WWSSN station in Kabul (KBL). Traces have not been normalized and relative amplitudes are correct. Arrows indicate group velocities on each trace. Top line is from anomalous event A, 11° away; middle line is from anomalous event B, 6° away; and bottom line is from underground explosion G, 17° away. Strong arrival at about 3.0 km/s on explosion record is short-period branch of fundamental mode.

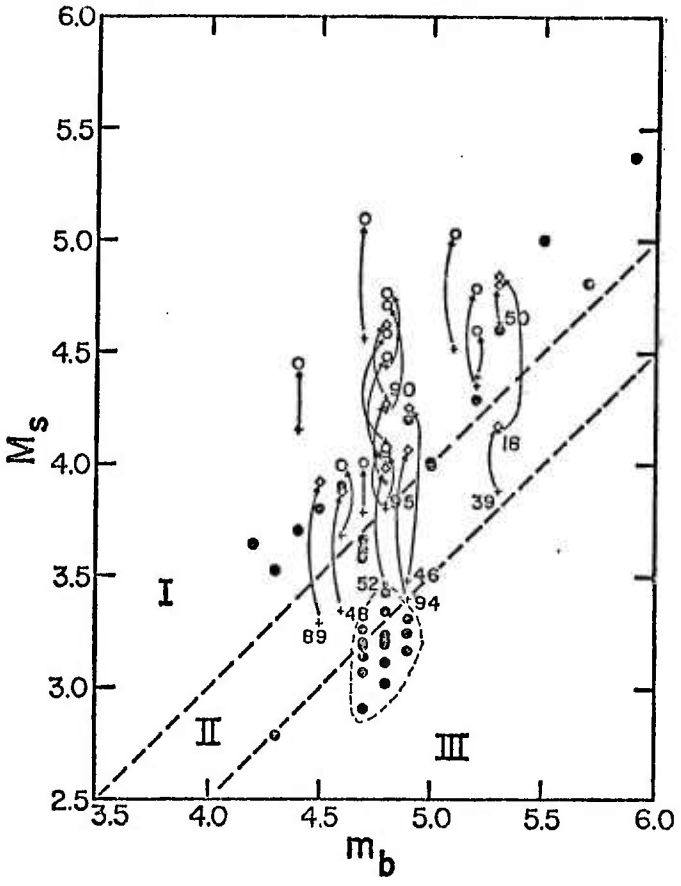


FIG. 26 $M_s - m_b$ diagram summarizing analysis of Tibetan anomalous events. Arrows and diamonds show increase in $M_s$ values when observations of higher-mode Rayleigh waves are included, with (+) indicating original $M_s$ value. Arrows and open circles show increase in $M_s$ values when observations of Love waves are included. Dashed line contains all reported events of the 1968–1969 swarm

TABLE 3

MAGNITUDES, ORIGIN TIME AND LOCATION OF ANOMALOUS EVENTS AND EXPLOSIONS*

| Event | Date (m d yr) | Origin Time (h:m:s) | Latitude (N|E) | Longitude | Depth | $m_b$ | $M_s$† | $M_c$* |
|---|---|---|---|---|---|---|---|---|
| A‡ | 05 01 69 | 04:00:08.7 | 44.0 | 77.9 | 53 | 4.9 | 2.9 | 3.9 |
| B‡ | 12 09 69 | 13:41:09.0 | 40.1 | 70.7 | 33 | 4.9 | 3.6 | 4.1 |
| C‡ | 07 01 68 | 19:14:54.7 | 44.0 | 79.3 | 33 | 4.8 | 2.9 | 3.9 |
| D§ | 10 24 71 | 08:49:04.6 | 28.2 | 87.2 | 44 | 4.8 | 2.8 | (3.8) |
| E§ | 11 24 71 | 08:23:24.6 | 38.7 | 73.3 | 33 | 4.6 | 2.8 | 3.6 |
| F§ | 12 04 71 | 08:38:00.7 | 27.9 | 87.9 | 32 | 4.9 | 3.2 | 4.1 |
| G | 11 30 69 | 03:32:57.1 | 49.9 | 79.0 | 0 | 6.1 | 4.2 | 4.3 |
| H | 03 22 71 | 04:32:57.7 | 49.8 | 78.2 | 0 | 5.8 | 4.1 | 4.1 |
| I | 11 02 72 | 01:26:57.5 | 49.9 | 78.8 | 0 | 6.2 | 3.9 | 4.1 |

* Hypocentral data from NEIC.

† All $M_s$ values have been recomputed to a common scale and may not be identical to original references.

‡ Original reference: Landers (1972).

§ Original reference: Nuttli and Kim (1975).

where T is the period of the maximum amplitude A, B'(Δ) is distance correction from Marshall and Basham (1972), and $T_0$ is the reference period of 10s. This formula should be modified if used in areas other than central Asia, because B'(Δ) and the mode correction factor, log 7.5, may vary from region to region.

The ratio of surface-to body-wave magnitude, $M_s:m_b$, provides one of the principal means of distinguishing earthquakes from underground explosions (e.g. Evernden, 1969; Liebermann and Pomeroy, 1969). Explosions tend to be less efficient generators of surface waves, with $M_s$ less than $[m_b - 1.5]$. In contrast, $M_s$ for most shallow earthquakes is greater than or equal to $[m_b - 1.0]$ (Conference Committee on Disarmament, 1972). However, there are a few "anomalous" earthquakes which have explosion-like $M_s:m_b$ ratios, or fall between the earthquake and explosion population, i.e. $[m_b - 1.0] > M_s \geq [m_b - 1.5]$, and thus are statistically indistinguishable from explosions. Examples of anomalous earthquakes in central Asia have been presented by Landers (1972), the Conference of the Committee on Disarmament (1972), Douglas et al. (1974) and Nuttli and Kim (1975).

The long-period, vertical component of motion for two anomalous earthquakes and an underground explosion are shown in Figure 25 as recorded at the WWSSN station in Kabul, Afghanistan (KBL, Figure 20). Locations and magnitudes are given in Table 3. The signal from event A, an earthquake in Kazakh, shown at the top of the figure, happens to be superimposed on the Rayleigh wave train from a much larger earthquake in the Tonga region. Although the high-frequency Rayleigh wave from the Kazakh event is clearly visible, it is impossible to obtain a reliable estimate of the 20s signal level of the smaller earthquake. Event A can be seen at several other stations in central Asia, but in each case, the surface waves from Tonga interfere. All of the anomalous events are small, making it difficult to measure the spectrum over a period range broad enough to avoid frequency-dependent source effects, even when there is no interfering signal. For event A, $M_s$ has to be based on signals of period 7 to 8s, yielding an estimated magnitude of 2.9, well within the explosion population. However, as Landers (1972) pointed out, the amplitude of the higher mode arrival at about 3.4 km/s is equal to or greater than the amplitude of the fundamental mode. The revised estimate of surface wave magnitude, $M_s^h = 3.9$, places the event in the earthquake population (Table 3). Another similar event located nearby (C in Table 3) is also removed from the anomalous category by using $M_s^h$. The number of observations on which $M_s^h$ is based is listed in the last column of Table 3.

Unlike events A and C, for which no long-period surface waves could be detected, event B generated 20s Rayleigh waves which could easily be measured at KBL (2nd line in Figure 25). The $M_s:m_b$ relation for event B falls between the earthquake and explosion populations, but again, the amplitude of the higher mode restores it to the earthquake group. $M_s^h$ also allows two of the anomalous earthquakes listed by Nuttli and Kim (1975) to be classified as normal earthquakes (events E and F in Table 3). Event F is unusual in that 40- to 60s period Rayleigh waves are clearly visible at the WWSSN station NDI and the high-gain, long-period station at Chiang

Mai, Thailand (CHG), even though very little fundamental mode Rayleigh or Love wave signal with period less than 30s can be seen at any station. The higher mode from this event travels with a group velocity of about 3.8 km/s, in contrast to the crustal velocities observed for other events. The mantle-like velocity of the higher mode and the long-period character of the fundamental mode suggests that the earthquake occurred deep within the Himalayan crust, perhaps at a depth of 70 km or more. $M_S$ based on the 60s period waves is about 4.0, in reasonably good agreement with $M_S^h$. Event D occurred in nearly the same location as event F, but was too small to generate an observable higher mode. The fundamental mode could, however, be detected at the CHG high-gain station where it was recorded with the same waveform at about half the amplitude of event F. I suggest that event D also occurred deep within the Himalayan crust and, by analogy with event F, should be assigned an $M_S^h$ of about 3.8. Other examples of higher modes from anomalous earthquakes in the Tibetan area are presented by Tatham et al. (1975) and the effect of using $M_S^h$ instead of $M_S$ is shown in Figure 26.

If the higher mode magnitude scale is correct, $M_S^h$ should be equal to $M_S$ for very shallow earthquakes or underground explosions. Although there are as yet no known explosions within an area with a 70 km thick crust, an attempt was made to test the validity of the scale using signals from the Soviet nuclear test site in eastern Kazakh (Figure 20). One effect of a thinner crust is to reduce the period of the higher modes trapped in the crustal wave guide. As can be seen in the bottom trace in Figure 25, the maximum period of the higher mode generated by the explosion is only about 5s. $M_S^h$ for three explosions at the site, events G, H and I in Table 3, is 0.05 to 0.15 units larger than $M_S$. This discrepancy is not large and may be due to the differences in crustal structure between the test site and the locations of the anomalous earthquakes for which the scale was designed.

## F. FOCAL MECHANISMS OF SMALL MAGNITUDE EVENTS

Tatham and Savino (1973) described a surface wave technique for studying the focal mechanisms of small magnitude events at teleseismic distances. The method consists of comparing observed amplitudes of long-period Rayleigh and Love waves with radiation patterns of focal mechanisms consistent with the previously determined tectonic regime of a certain region. It is important to note that in using this method we do not determine focal mechanisms, per se, but rather discriminate between different types of mechanisms thought to be prevalent in a region.

In the study of Tatham and Savino (1973) the relative amplitudes of Rayleigh and Love waves with periods between 10 and 50 seconds were determined for some 60 swarm-type events, assumed to be shallow (h<15 km), that occurred near the Delfin basin in the northern Gulf of California. These surface waves were recorded at the new high-gain station at Albuquerque, New Mexico (ALQ). The bathymetry and seismicity of the northern Gulf of California suggest that faulting is occurring at short spreading centers (dip-slip faulting) and along transform faults (strike-slip faulting). The radiation patterns for Love and Rayleigh waves corresponding to the above faulting patterns for the northern Gulf of California are

schematically illustrated in Figure 27. All of these patterns were computed assuming double-couple sources and shallow focal depths. The position of the nodes in the radiation patterns for strike-slip faulting are independent of focal depth, but there are changes in the absolute amplitude of the lobes, especially for Rayleigh waves, with variations in focal depth. The dip-slip radiation patterns are for a pure dip-slip mechanism with the fault plane $15^{0}$ from vertical and zero focal depth. It is important to note that these dip-slip patterns change significantly with increasing focal depth, even to a depth as shallow as 33 km. That is, as depth increases for dip-slip mechanisms, the number of nodes and the number and amplitude of lobes, change. However, the amplitudes of the surface waves, especially Rayleigh waves, tend to decrease as depth increases, an effect that is especially pronounced for these dip-slip mechanisms. Further, the amplitudes of surface waves generated by near-vertical dip-slip faulting tend to be small at all focal depths. The reader is referred to the paper by Tatham and Savino (1973) for more detailed arguments concerning the focal depths of the swarm events included in this study.

The near optimum azimuthal position of the high-gain seismograph station ALQ, with respect to the radiation patterns shown in Figure 27, provides for the possibility of discriminating between the two possible focal mechanisms assumed for the northern Gulf of California. For normal faulting on a spreading center, surface waves radiated on the azimuth of ALQ should be weak and of approximately equal amplitude distribution in both Love and Rayleigh waves. For strike-slip mechanisms, Love waves should be of much greater amplitude than Rayleigh waves. Figure 28 (a-b) shows examples of the relative excitation of Rayleigh and Love waves by two swarm events recorded on the 3-component high-gain seismographs at ALQ. Figures 28a and 28c show the three orthogonal components of each record segment normalized to a common magnification for each event. It is especially evident that the horizontal Love-wave motion dominates over the vertical motion. Further, the observed vertical motion does not have the character of fundamental Rayleigh waves, and may possibly be due to higher modes. Figures 28b and 28d illustrate the result of a rotation of the horizontal components into equivalent radial and transverse traces. Here the Love-wave motion of the transverse component is clearly much greater than the Rayleigh-type motion that would be observed on the vertical and radial components. In addition, the radial motion shows the same lack of fundamental Rayleigh-wave character as that observed for the vertical motion. These few examples demonstrate that Love waves are indeed the dominant surface waves observed at ALQ and from this it was concluded that strike-slip was probably the dominant faulting mechanism.

In total, surface waves from 60 events identified as being part of this swarm were observed at ALQ. In several cases, Love waves an order of magnitude smaller than those in Figure 28a and b, an $m_b = 4.2$ event, were recorded demonstrating the value of the horizontal components and how they enhance the detection capabilities of a single seismograph station.

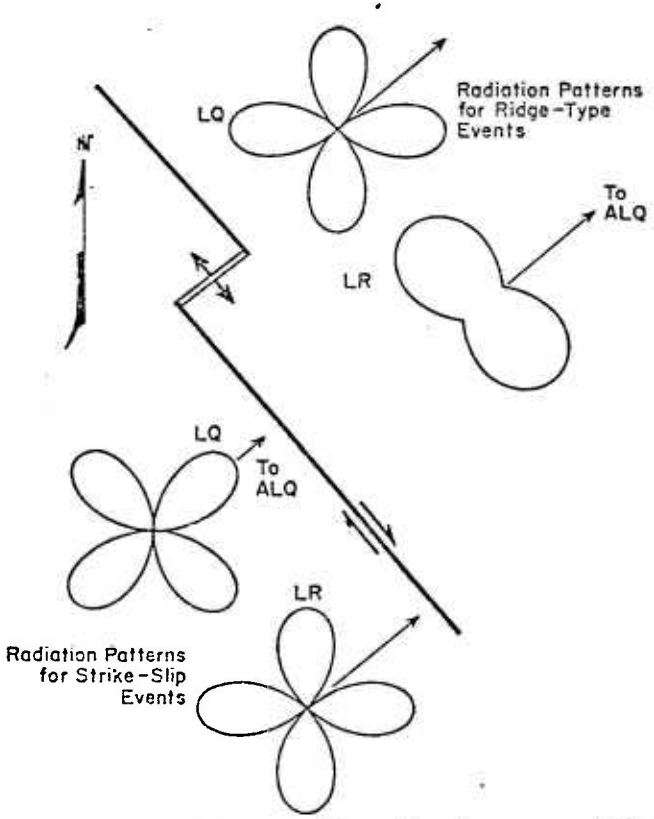


Fig. 27. Schematic representation of surface wave radiation patterns for faulting mechanisms anticipated in the northern Gulf of California. Note the optimum azimuthal position to ALQ for discriminating between the two types of faulting.

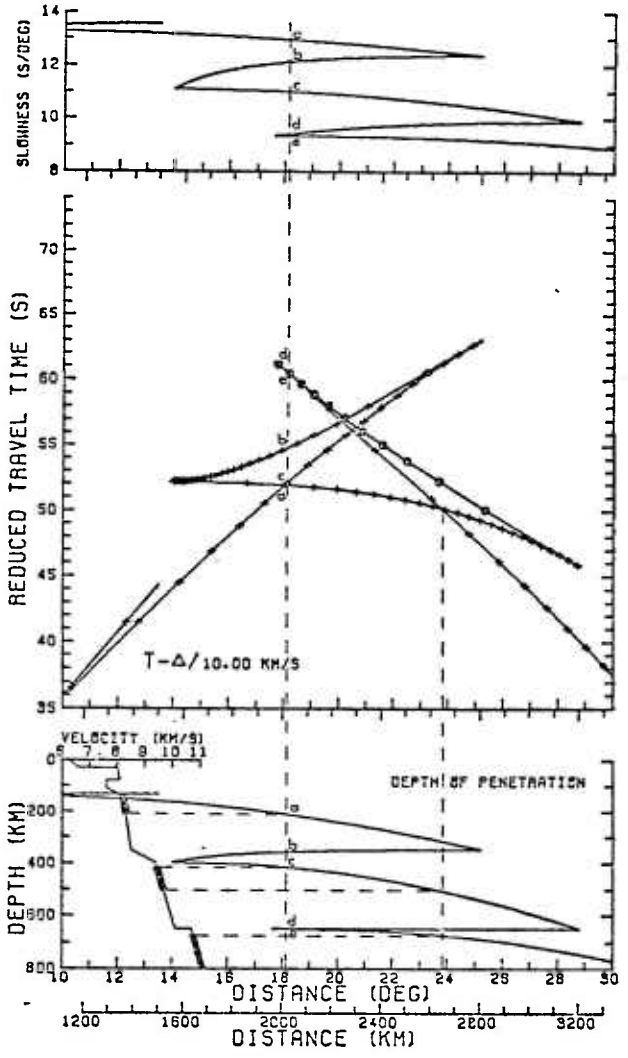


Figure 29 Hypothetical upper mantle model showing relationship between velocity, travel time and slowness.

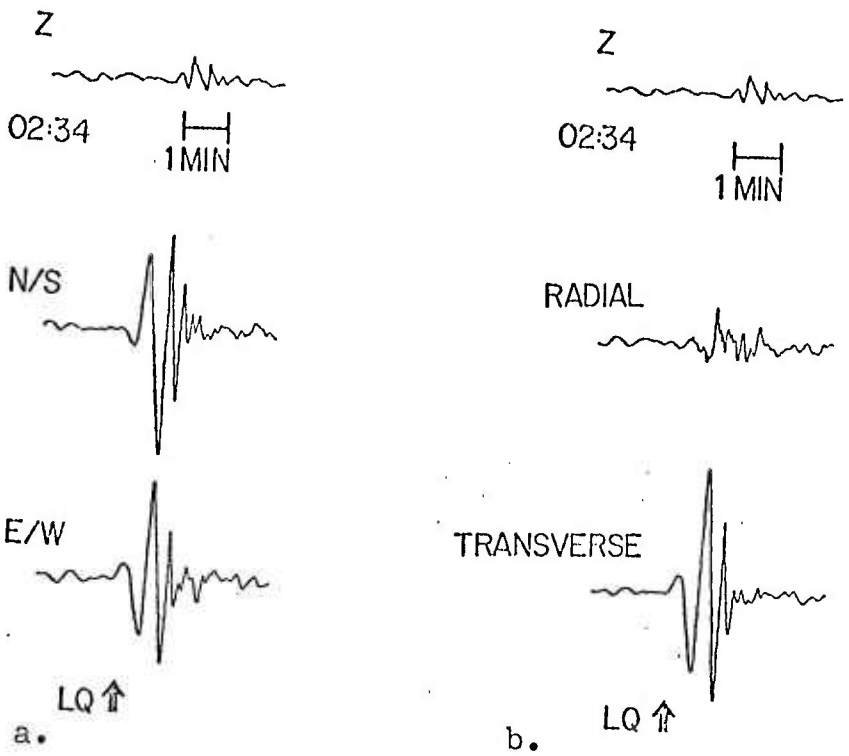


Figure 28 a) Portions of ALQ seismograms showing surface waves from two swarm events. Recordings start at 02:34, with all components normalized to the same magnification.

b) The same data with horizontal components rotated into equivalent radial and transverse components. Note strong Love-wave motion on transverse component.

c) Same as Figure 2a - for portion of traces starting at 04:49.

d) Same as Figure 2b - for portion of traces starting at 04:49.

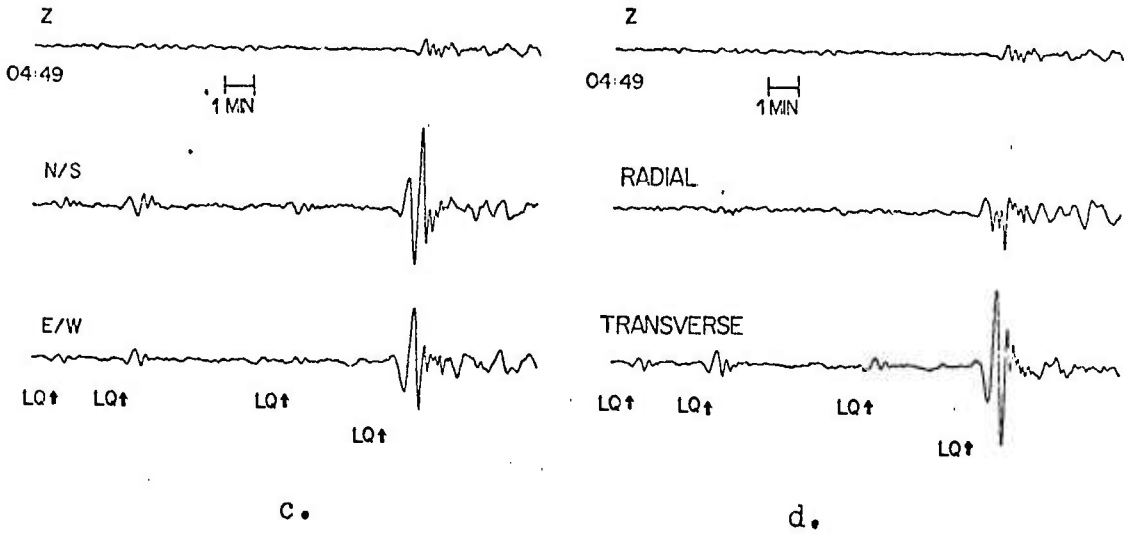

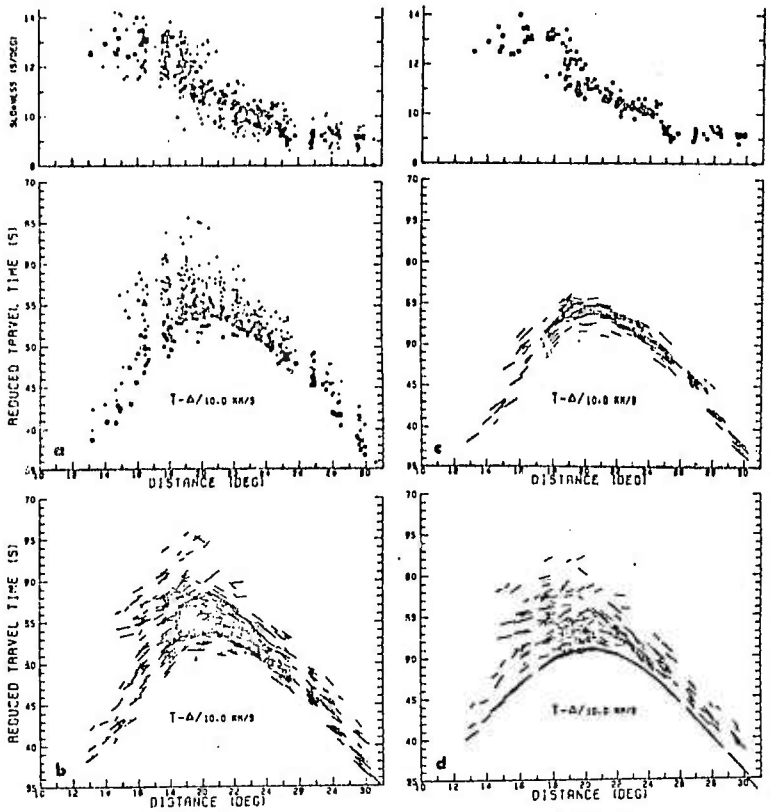


Figure 30 a) WRA travel time and slowness data. Squares indicate first arrivals. b) Combined travel time and slowness data. Slope lines plotted with slope of measured slowness. Short vertical lines indicate first arrivals. c) First arrival data only. d) Travel times adjusted so that first arrivals fall on Herrin et al.[11] travel time curve. (From Simpson, Mereu and King[5])

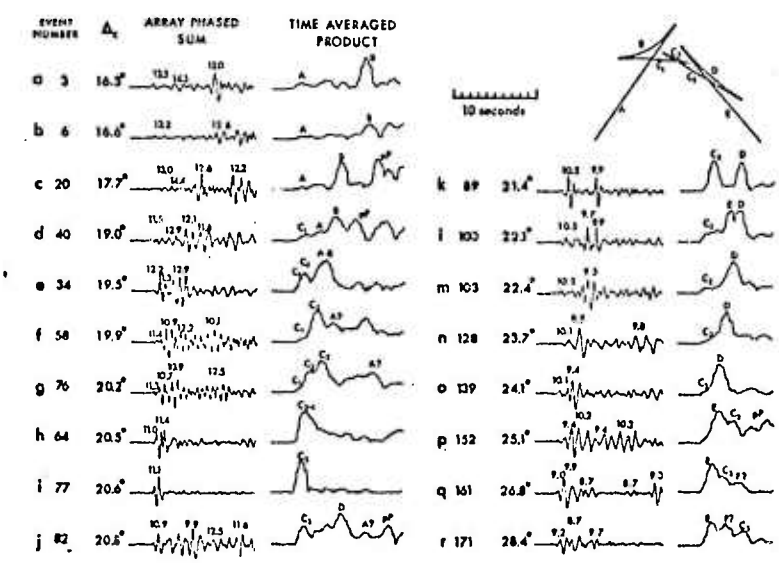


Figure 31 Examples of processed records. Numbers over array-phased-sum traces are observed slowness values (s/deg). (From Simpson, Mereu and King[5])

## G. PULSE DISTORTION IN BODY WAVES

Many seismic body waves are associated with rays which are not minimum travel time paths. Such arrivals contain pulse deformation due to a phase shift in each frequency component. For sufficiently high frequencies, the phase shift is $\pi/2$ and frequency independent. Hence, the original waveform is related to the distorted pulse via Hilbert transformation. The distorting effect of a frequency-independent phase shift is successfully observed in seismograms from events in several regions. The data examined are long period (T>9 seconds) and were taken from the high-gain stations and the WWSSN. They include deep earthquakes (depth>500 km), in which a series of well separated S phases (S, sS, SS and sSS) are available. These show that the waveform of SS, which has been distorted in propagation through the Earth, can be derived from the waveform of sS, which is not distorted. SS and sS form a Hilbert transform pair. Shallow events, in which multiple S phases overlap, also exhibit behavior predicted by phase distortion. Rays critically reflected or refracted at a discontinuity in the Earth also suffer a constant phase shift, which in general can have any value. An important case is SKKS: its undistorted wave form resembles that of SKS, which has a minimum travel time path.

Without exception, all the distorted waveforms bear little or no resemblance to the original waveform. That is, neither the first arrival of energy nor the subsequent relative position of peaks and troughs on a distorted waveform appear at the ray theoretical times. Thus, T-$\Delta$ curves constructed by choosing arrival times to correspond to the first arrival of energy may be biased. Similarly, doubt is cast on differential travel times chosen from first motions, or from averaging several points on what appear to be corresponding peaks and troughs of two waveforms. Some of the rays most important to seismology, in which the distortion phenomenon occurs, include P and S (where $d^2T/d\Delta>0$), $PKP_{AB}$, PP, SS, and SKKS. We find that removal of phase distortion in the data is computationally straightforward, and the resulting waveform may be exploited to full advantage in correctly picking arrival times.

## H. USE OF SEISMOGRAPH ARRAYS IN DETERMINING EARTH STRUCTURE

Seismic arrays can be considered in three modes of operation:

1) S/N improvement. The insertion of delays between sensors creates an azimuth and slowness filter. Since, in general, distance is a unique function of slowness, this process enhances signals originating in one location with respect to those from another. The appropriate delays can be determined directly by the array, or, for a specific source location, they can be approximated from the calculated azimuth and standard tables of slowness as a function of distance.

2) Determination of seismic parameters. Using signals from events in known locations, values of azimuth deviations and of slowness as a function of distance can be determined.

3) Event location. If a table of slowness as a function of distance is available, either from 2) above or from standard tables, measured values of slowness and azimuth can be used to specify the azimuth and distance to, and hence the location of, the source of the recorded signal.

It is in the second mode of operation that arrays are able to provide the most useful information about the internal structure of the Earth.

The first distance derivative of the travel time curve ($dT/d\Delta$) can be shown to equal the seismic ray parameter "p" and it is this parameter, as a function of distance (see equation 2) which is required in order to derive a velocity-depth distribution. Until recent years $dT/d\Delta$ could only be obtained by smoothing observed travel time data and finding the slope of the smoothed curve. With the advent of modern seismic arrays, it is now possible to measure $dT/d\Delta$ directly and independently of absolute time, thus removing many of the errors associated with the earlier technique.

The true velocity ($v_t$) at the maximum depth of penetration ($d_p$) for a given ray is related to the apparent velocity ($v_a$) at the Earth's surface (radius $R_E$) by

$$v_t = \frac{v_a (R_E - d_p)}{R_E} \qquad (1)$$

It is obvious from (1) that the slope ($dT/d\Delta$, proportional to the inverse of $v_a$) and hence the shape, of any part of the travel time curve is determined by the velocity at the maximum depth of penetration for the rays arriving over that part of the curve. Conversely, if the apparent velocity at the surface is known as a function of distance, the true velocity at depth can be found by determining the corresponding depths of penetration as a function of distance. This is done using the following solution to the Abel integral equation

$$\ln \frac{R_E}{(R_E - d_p)} = \frac{1}{\pi} \int_0^{\Delta_1} \cosh^{-1} \frac{p}{p_1} \, d\Delta \qquad (2)$$

where $p = dT/d\Delta$ or slowness, and the subscript 1 refers to rays which have reached a maximum depth of penetration $d_p$.

When the apparent velocity (or slowness) at the surface (i.e. $v_a$ or $dT/d\Delta$) is known as a function of distance ($\Delta$) the right-hand-side of (2) can be evaluated, determining $d_p$ and, hence, from (1) the velocity at $d_p$. By evaluating the integral for various values of $\Delta$, different depths are sampled, allowing a velocity-depth distribution to be determined.

Figure 29 shows the travel time curve and related parameters for a hypothetical upper mantle velocity model. Slowness ($dT/d\Delta$, in s/deg), reduced travel time ($T-\Delta/10$ km/s, in s) and depth of penetration (in km) are shown as a function of distance ($\Delta$, in both km and deg). Velocity (in km/s) is given as a function of depth (in km).

This presentation stresses the importance of later arrivals in determining velocity structure. The vertical lines in Figure 29 at the cross-over distances near 18° and 24° show that the first arrival portions of the travel time curve correspond to rays which reach their maximum depths of penetration over a very limited range. Between depths of 200 and 700 km, first arrivals in this model correspond to a total depth interval of only 100 km. Depths near the two discontinuities at 400 and 650 km are always related to later arrivals. Thus, if the details of later arrivals are unknown, much of the velocity distribution is beyond the scope of the data.

Figure 30 shows the complete travel time and slowness data used in the WRA upper mantle study of Simpson, Mereu and King (1974). If only the travel time or slowness data in Figure 30a were used, it would be difficult to interpret any of the later arrivals. However, when the travel time and slowness data are combined, as shown in Figure 30b and d, later arrivals, especially between 20° and 25° (branch D in Figure 31), clearly show a major triplication. When individual records are considered, the usefulness of slowness information is even more apparent. Examples k to o in Figure 31 show that second arrivals such as that in Figure 31k appear as distinct phases only near 21°-22°. If only travel times were used, these arrivals could easily have been misinterpreted as belonging to the later arrival extension of the A branch (Figure 31, insert). As Figure 30 indicates, however, slowness determinations definitely place these arrivals on the D branch.

The basic information required to derive velocity as a function of depth within the Earth is the slope of the travel time curve ($dT/d\Delta$, or slowness) as a continuous function of distance. Regions of high velocity gradient, such as the transitions in the upper mantle near 400 km and 650 km, cause triplications in the travel time curve, so that later arrivals must be studied to obtain a complete slowness-distance relationship. The use of seismograph arrays to determine slowness not only allows this parameter to be determined independently of absolute travel time, but also aids in the picking of later arrivals and in correlating them with particular branches of the travel time curve.

# REFERENCES


Archambeau, C.B., 1968, General theory of elastodynamic source fields, Rev. Geophys., 6, 241-288.

Archambeau, C.B and Flinn, E.A., Automated analysis of seismic radiation for source characteristics, Proc. IEEE, 53, 1876, 1965.

Brune, J.N., 1970, Tectonic stress and the spectra of seismic shear waves from earthquakes, J. Geophys. Res., 75, 4997-5009.

Choy, G. and McCamy, K., Enhancement of long-period signals by time-varying adaptive filters, J. Geophys. Res., 78, 3505-3511.

Conference of the Committee on Disarmament, 1972, A review of current progress and problems in seismic verification, CCS, 388 pp.

Douglas, A., Hudson, J.A., Marshall, P.D., and Young, J.B., 1974, Earthquakes that look like explosions, Geophys. J. R. Astr. Soc., 36, 227-233.

Evernden, J.F., 1967, Magnitude determination at regional and near-regional distances in the United states, Bull. Seism. Soc. Am., 57, 591.

Evernden, J.F., 1969, Identification of earthquakes and explosions by use of teleseismic data, J. Geophys. Res., 74, 3828-3856.

Evernden, J.F., Best, W.J., Pomeroy, P.W., McEvilly, T.V., Savino, J.M. and Sykes, L.R., 1971, Discrimination between small-magnitude earthquakes and explosions, J. Geophys. Res., 76, 8042.

Fix, J.E., 1973, Theoretical and observed noise in a high-sensitivity long-period seismograph, Bull. Seism. Soc. Am., 63, 1974-1998.

Flinn, E.A., Signal analysis using rectilinearity and direction of particle motion, Proc. IEEE, 53, 1874, 1965.

Gutenberg, B., 1945, Amplitudes of surface waves and magnitudes of shallow earthquakes, Bull. Seism. Soc. Am., 35, 3.

Hasselmann, K., 1963, A statistical analysis of the generation of microseisms, Rev. Geophys., 1, 177-210.

Haubrich, R.A. and McCamy, K., 1969, Microseisms: Coastal and pelagic sources, Rev. Geophys., 7, 539-571.

Herrin, E., Tucker, W., Taggart, J.N., Gordon, D.W., and Lobdell, J.L., Estimation of surface-focus P travel times, in 1968 Seismological Tables for P Phases, (chairman, E. Herrin), Bull. Seism. Soc. Am., 58, 1273, 1968.

Herron, T.J., Tolstoy, I., and Kraft, D.W., 1969, Atmospheric pressure background fluctuations in the mesoscale range, J. Geophys. Res., 74, 1321-1329.

Landers, T., 1972, Some interesting central Asian events on the $M_S$:$m_b$ diagram, Geophys. J. R. Soc., 31, 329-339.

Landismann, M., Dziewonski, A., and Sato, Y., 1969, Recent improvements in the analysis of surface wave observations, Geophys. J. R. Astr. Soc., 17, 369-403.

Larson, R.J., Craine, L.B., Thomas, J.E., and Wilson, C.R., 1971, Correlation of winds and geographic features with production of certain infrasonic signals in the atmosphere, Geophys. J. R. Astr. Soc., 26, 201-214.

Liebermann, R.C. and Pomeroy, P.W., 1969, Relative excitation of surface waves by earthquakes and underground explosions, J. Geophys. Res., 74, 1575-1590.

Linde, A.T., and Sacks, I.S., 1971, Errors in the spectral analysis of long-period seismic body waves, J. Geophys. Res., 76, 3326-3336.

Longuet-Higgins, M.S., 1950, A theory of the origin of microseisms, Phil. Trans. R. Soc. London, A, 243, 1-35.

Marshall, P.D. and Basham, P.W., 1972, Discriminations between earthquakes and underground explosions employing an improved $M_S$ scale, Geophys. J. R. Astr. Soc., 28, 431-458.

McDonald, J.A., Douze, E.J., and Gerren, E.T., 1971, The structure of atmospheric turbulence and its application to the design of pipe arrays, Geophys. J. R. Astr. Soc., 26, 71-82.

Molnar, P., Savino, J., Sykes, L.R., Liebermann, R.C., Nade, G. and Pomeroy, P.W., 1969, Small earthquakes and explosions in western North America recorded by new high-gain, long-period seismographs, Nature, 224, 1268.

Nuttli, O.W. and Kim, S.G., 1975, Surface-wave magnitudes of Eurasian earthquakes and explosions, Bull. Seism. Soc. Am., 65, 693-709.

Oliver, J., 1962, A world wide storm of microseisms with periods of about 27 seconds, Bull. Seism. Soc. Am., 52, 507-517.

Priestly, J.T., 1966, Correlation studies of pressure fluctuations on the surface beneath a turbulent boundary layer, N.B.S. Report 8442, U.S. Dept. of Commerce, National Bureau of Standards.

Savino, J.M. and Rynn, J.M.W., 1972, Quasi-static loading of the earth by propagating air waves, J. Geophys. Res., 77, 5033-5041.

Savino, J., Sykes, L.R., Liebermann, R.C. and Molnar, P., 1971, Excitation of seismic surface waves with periods of 15 to 70 seconds for earthquakes and underground explosions, J. Geophys. Res., 76, 8003.

Savino, J.M., McCamy, K., and Hade, G., 1972, Structures in earth noise beyond twenty seconds - a window for earthquakes, Bull. Seism. Soc. Am., 62, 141-176.

Savino, J.M., Murphy, A.J., Rynn, J.M.W., Tatham, R., Sykes, L.R., Choy, G.L., and McCamy, K., Results from the high-gain long-period seismograph experiment, Geophys. J. R. Astr. Soc., 31, 179, 1972b.

Sax, R.L., and Mims, C.M., Rectilinear motion detection, Rep. 118, 15 pp., Seismic Data Lab., Alexandria, Va., 1965. (ARPA order 624, AF contract 33(657)12447, March 1965).

Simons, R.S., A surface wave particle motion discrimination process, Bull. Seism. Soc. Am., 58, 629, 1968.

Simpson, D.W., Mereu, R.F. and King, D.W., An array study of P wave velocities in the upper mantle transition zone beneath northeastern Australia, Bull. Seism. Soc. Am., (in press), 1974.

Sorrells, G.G., 1971, A preliminary investigation into the relationship between long-period seismic noise and local fluctuations in the atmospheric pressure field, Geophys. J. R. Astr. Soc., 26, 71-82.

Sorrells, G.G. and Douze, E.J., 1974, A preliminary report on infrasonic waves as a source of long-period seismic noise, (in press).

Tatham, R.H. and Savino, J.M., Faulting mechanisms for two oceanic earthquake swarms, J. Geophys. Res., 79, 2643-2691.

Tatham, R.H., Forsyth, D.W., and Sykes, L.R., 1975, Tectonics of the eastern Himalayas and occurrence of anomalous seismic events, submitted to Geophys. J. R. Astr. Soc.

## III. PAPERS PUBLISHED UNDER THIS CONTRACT


Choy, G. and K. McCamy, Enhancement of long-period signals by time-varying adaptive filters, J. Geophys. Res. 78, 3505-3511.

Choy, G. L. and P. L. Richards, Pulse distortion and Hilbert transformation in multiply reflected and refracted body waves, Bull. Seism. Soc. Amer. 65, 55-70, 1975.

Forsyth, D. W., Higher-mode Rayleigh waves as an aid to seismic discrimination, Bull. Seism. Soc. Amer. in press, 1976.

Murphy, A. J., K. McCamy, and J. M. Savino, Novel observations of long-period (30 to 60 sec) microseisms, submitted to J. Geophys. Res., 1976.

Murphy, A. J. and J. M. Savino, A comprehensive study of long-period (20 to 200 seconds) earth noise at the high-gain world wide seismograph stations, Bull. Seism. Soc. Amer. 65, 1827-1862, 1975.

Murphy, A. J. and J. M. Savino, Attenuation of long-period earth noise with depth, submitted to J. Geophys. Res., 1976.

Murphy, A. J., J. Savino, J. M. W. Rynn, G. L. Choy, and K. McCamy, Observations of long-period (10-100 sec) seismic noise at several world wide locations, J. Geophys. Res. 77, 5012-5049.

Savino, J. M. and J. M. W. Rynn, Quasi-static loading of the Earth by propagating air waves, J. Geophys. Res. 77, 5033-5049, 1972.

Savino, J., K. McCamy and G. Hade, Structures in earth noise beyond twenty seconds - a window for earthquakes, Bull. Seism. Soc. Amer. 62, 141-176.

Savino, J. M., A. J. Murphy, J. M. W. Rynn, R. Tatham, L. R. Sykes, G. L. Choy and K. McCamy, Results from the high-gain long-period seismograph experiment, Geophys. J. R. Astr. Soc. 31, 179-203, 1972.

Savino, J., L. R. Sykes, R. C. Liebermann, and P. Molnar, Excitation of seismic surface waves with periods of 15 to 70 seconds for earthquakes and underground explosion J. Geophys. Res. 76, 8003-8020, 1971.

Simpson, D. W., The use of seismograph arrays in determining earth structure, in Exploitation of Seismograph Networks, K. G. Beauchamp, ed., NATO Advanced Study Institutes Series E, No. 11, 1975.

Tatham, R. H., D. W. Forsyth, and L. R. Sykes, The occurrence of anomalous seismic events in eastern Tibet, Geophys. J. R. Astr. Soc. in press, 1976.

Tatham, R. H. and J. M. Savino, Faulting mechanisms for two oceanic earthquake swarms, J. Geophys. Res. 79, 2643-2691.

# REPORT DOCUMENTATION PAGE

READ INSTRUCTIONS BEFORE COMPLETING FORM

1. REPORT NUMBER: AFOSR-TR-76-0932
2. GOVT ACCESSION NO.
3. RECIPIENT'S CATALOG NUMBER
4. TITLE (and Subtitle): Long-Period Seismological Research Program.
5. TYPE OF REPORT & PERIOD COVERED: Final rept. 15 Mar 71-30 Apr 76
6. PERFORMING ORG. REPORT NUMBER
7. AUTHOR(s): Drs. Lynn R. Sykes and Donald W. Forsyth
8. CONTRACT OR GRANT NUMBER(s): F44620-71-C-0082; ARPA Order-1827
9. PERFORMING ORGANIZATION NAME AND ADDRESS: Columbia University, Lamont-Doherty Geological Observatory, Palisades, New York 10964
10. PROGRAM ELEMENT, PROJECT, TASK AREA & WORK UNIT NUMBERS: A01827-12&17; 62701E
11. CONTROLLING OFFICE NAME AND ADDRESS: ARPA, 1400 Wilson Blvd., Arlington, VA 22209
12. REPORT DATE: 30 June 1976
13. NUMBER OF PAGES: 58
14. MONITORING AGENCY NAME & ADDRESS (if different from Controlling Office): AFOSR/NP, Bolling AFB, Wash DC 20332
15. SECURITY CLASS. (of this report): unclassified
15a. DECLASSIFICATION/DOWNGRADING SCHEDULE
16. DISTRIBUTION STATEMENT (of this Report): Approval for public release: distribution unlimited
12 63p.
17. DISTRIBUTION STATEMENT (of the abstract entered in Block 20, if different from Report)
18. SUPPLEMENTARY NOTES: Tech, other
19. KEY WORDS (Continue on reverse side if necessary and identify by block number)

Long-period
Ogdensburg, New Jersey
High-gain seismic stations
Surface waves
Higher modes
Discrimination
Central Asia
Earth noise
Signal enhancement

20. ABSTRACT (Continue on reverse side if necessary and identify by block number)

During the first year of the subject contract, five high-gain long-period (HGLP) seismograph stations were maintained and a sixth station was installed and maintained. During the second year, responsibility for maintenance was transferred to the Albuquerque Seismological Center. In succeeding years, Lamont-Doherty continued operating the high-gain station at Ogdensburg, New Jersey (OGD). Research completed under this contract



404 497 LB

included investigation into the characteristics of long-period earth noise, the detection capabilities of the high-gain stations, digital signal enhancement techniques, and new methods of distinguishing earthquakes from underground explosions, as well as several studies in general seismology using high-gain data.

A detailed study of earth noise at all 11 HGLP sites found that the spectra of earth noise at each site are characterized by a minimum in the period range 25 to 45 seconds. The level of earth noise recorded by vertical seismographs is independent of local meteorological conditions, but at shallow sites the earth noise levels recorded by horizontal seismographs exhibit a diurnal cycle associated with daily variations of atmospheric turbulence. The horizontal earth noise associated with atmospheric turbulence is attenuated by overburden to about 10% of the surface noise level at a depth of about 150 m.

An evaluation of the detection capabilities of the HGLP stations showed that surface waves could be observed for 90% of the reported events of $m_b$ 4.2 or larger which occurred within 30° of a station. At distance ranges of 80° to 100°, the detection threshold increases to about $m_b$ 4.7. Roughly half of the 10% not observed are masked by the coda of earlier larger events. The thresholds are expected to be lowered by about 0.2 units if digital processing techniques, such as time-varying adaptive filters, are applied. Polarization and azimuthal filters are capable of a signal-to-noise enhancement of more than 6 db for signals from small events. These filters have proved to be more effective than passive techniques or matched filtering.

A new surface wave magnitude scale based on the amplitude of higher-mode Rayleigh waves was developed and applied to earthquakes and explosions in central Asia. Several anomalous events in central Asia, which are characterized by unusually low $M_S$:$m_b$ ratios and hence could be suspected to be nuclear explosions, are reclassified as earthquakes when the new, higher-mode scale, $M_S^h$, is employed. The focal depth and mechanism of these anomalous events apparently causes poor excitation of the fundamental mode Rayleigh wave without significantly affecting the amplitude of the higher mode. Elimination of these source related factors from traditional $M_S$:$m_b$ discriminants is an essential tool for reliable discrimination between earthquakes and nuclear underground tests.

In other investigations, surface waves were used to study the focal mechanism of small magnitude events, the pulse distortion of body waves travelling non-minimum time paths was computed, and the use of seismograph arrays in determining earth structure was examined.